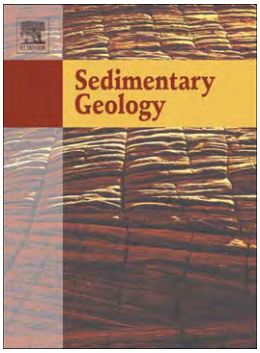

Depositional architecture of a mixed travertine-terrigenous system in a fault-controlled continental extensional basin (Messinian, Southern Tuscany, Central Italy)

Andrea Croci, Giovanna Della Porta, Enrico Capezzuoli

PII: S0037-0738(15)00247-X
DOI: doi: 10.1016/j.sedgeo.2015.11.007
Reference: SEDGEO 4939

To appear in: *Sedimentary Geology*

Received date: 15 July 2015
Revised date: 11 November 2015
Accepted date: 15 November 2015

Please cite this article as: Croci, Andrea, Della Porta, Giovanna, Capezzuoli, Enrico, Depositional architecture of a mixed travertine-terrigenous system in a fault-controlled continental extensional basin (Messinian, Southern Tuscany, Central Italy), *Sedimentary Geology* (2015), doi: 10.1016/j.sedgeo.2015.11.007

Depositional architecture of a mixed travertine–terrigenous system in a fault-controlled continental extensional basin (Messinian, Southern Tuscany, Central Italy)

Andrea Croci[a], Giovanna Della Porta[a], Enrico Capezzuoli[b]

[a] Earth Sciences Department, Milan University, 20133 Milan, Italy; andrea.croci@unimi.it

[b] Department of Physics and Earth Sciences, University of Perugia, 06100 Perugia, Italy

Highlights

- A facies analysis of continental carbonates and terrigenous deposits was conducted.
- The interplay between hydrothermal travertines and alluvial/colluvial deposits was demonstrated.
- The basin fill and depositional architecture of a continental extensional basin were studied.
- Extrinsic factors controlling the evolution of the sedimentary succession were determined.

ABSTRACT

The extensional Neogene Albegna Basin (Southern Tuscany, Italy) includes several thermogene travertine units dating from the Miocene to Holocene time. During the late Miocene (Messinian), a continental fault-controlled basin (of nearly 500-km^2 width) was filled by precipitated travertine and detrital terrigenous strata, characterized by a wedge-shaped geometry that thinned northward, with a maximum thickness of nearly 70 m. This mixed travertine–terrigenous succession was investigated in terms of lithofacies types, depositional environment and architecture and the variety of precipitated travertine fabrics.

Deposited as beds with thickness ranging from centimetres to a few decimetres, carbonates include nine travertine facies types: F1) clotted peloidal micrite and microsparite boundstone, F2) raft rudstone/floatstone, F3) sub-rounded radial coated grain grainstone, F4) coated gas bubble boundstone, F5) crystalline dendrite cementstone, F6) laminated boundstone, F7) coated reed boundstone and rudstone, F8) peloidal skeletal grainstone and F9) calci-mudstone and

microsparstone. Beds of terrigenous deposits with thickness varying from a decimetre to >10 m include five lithofacies: F10) breccia, F11) conglomerate, F12) massive sandstone, F13) laminated sandstone and F14) claystone.

The succession recorded the following three phases of evolution of the depositional setting: 1) At the base, a northward-thinning thermogene travertine terraced slope (Phase I, travertine slope lithofacies association, F1–F6) developed close to the extensional fault system, placed southward with respect to the travertine deposition. 2) In Phase II, the accumulation of travertines was interrupted by the deposition of colluvial fan deposits with a thickness of several metres (colluvial fan lithofacies association, F10 and F12), which consisted of massive breccias, adjacent to the alluvial plain lithofacies association (F11–F14) including massive claystone and sandstone and channelized conglomerates. Travertine lenses, of 2–3-m thickness, appeared intermittently alternating with the colluvial fan breccias. 3) In the third phase, the filled fault-controlled basin evolved into an alluvial plain with ponds rich in coated reed travertines, which record the influence of freshwater (travertine flat lithofacies association, F7–F9).

This study shows the stratigraphic architecture and sedimentary evolution of a continental succession, wherein the hydrothermal activity and consequent travertine precipitation were driven by the extensional tectonic regime, with faults acting as fluid paths for the thermal water. Fault activity created the accommodation space for travertine and colluvial fan accumulation. Erosion of the uplifted footwall blocks provided the source of sediments for the colluvial fan breccias, which alternated with the thermogene travertine precipitation. Climatic oscillations might have led to the recharge of the aquifer that fed the hydrothermal vents.

The studied continental succession in an extensional basin provides valuable information about the interplay between thermogene travertine and alluvial/colluvial deposition, which in turn might improve the understanding of similar fault-controlled continental depositional systems in outcrops and the subsurface.

Keywords

Thermogene travertines; alluvial deposits; continental rift basin; Messinian; Central Italy.

1. Introduction

Continental rift and strike-slip basins, such as the present-day examples of the East African Rift (McCall, 2010) and the Dead Sea Basin in the Middle East (Stein, 2001), present a variety of depositional environments and lithofacies including lacustrine carbonates, hydrothermal vent-related travertines as well as alluvial and fluvial deposits. In ancient cases of such fault-controlled basins, with deposition being influenced by varying rates of tectonic subsidence (Blair, 1987), mixed siliciclastic–carbonate successions occur alternately, as observed in the Jurassic–Lower Cretaceous of the Todos Santos Formation in Mexico (Blair, 1987), the Pliocene Ridge Basin in California (Link et al., 1978) and the Namibe Basin in southern Angola (Beglinger et al., 2012).

An important prerequisite for the development of travertine deposits is groundwater enriched in calcium and bicarbonate ions (Pentecost, 2005). Two classes of travertines are defined based on the two sources from which CO_2 can be derived: a) meteogene travertines are precipitated by groundwater enriched in meteoric carbon dioxide derived from soils and the atmosphere (Pentecost and Viles, 1994) and b) thermogene travertines are produced by thermally generated CO_2 (Pentecost, 2005). The signature of stable oxygen isotopes in meteogene travertines varies between −13‰ and 4‰ Vienna Pee Dee Belemnite (V-PDB), whereas the $\delta^{13}C$ values range from −12‰ to 4‰ V-PDB (Pentecost, 2005). In thermogene travertines, the oxygen isotope values range from −18‰ to −1‰ V-PDB, whereas carbon isotopes vary between −3‰ and 11‰ V-PDB (Pentecost, 2005). Some authors use the term ‘travertines’ exclusively to address continental carbonates precipitated by thermal water and the term ‘calcareous tufa’ to denote those carbonates associated with groundwater of ambient temperature (Pedley, 1990; Ford and Pedley, 1996; Capezzuoli et al., 2014). However, according to Jones and Renaut (2010), classifications based on the water

temperature or water sources do not consider the diagenetic processes, which is problematic in the case of ancient deposits. In this study, due to the sedimentological and geochemical results, the terminology proposed by Pentecost (2005) is used.

In the last decade, thermogene travertine deposits accumulated in rift basins have been increasingly studied as a valuable archive of information about Quaternary palaeoclimate, palaeohydrology and groundwater isotope geochemistry (Minissale et al., 2002a and b; Minissale, 2004; Faccenna et al., 2008; Kele et al., 2008, 2011; Özkul et al., 2014) and tectonics (Hancock et al., 1999; Altunel and Karabacak, 2005; Brogi et al., 2010). In addition, recent discoveries of Lower Cretaceous hydrocarbon reservoirs in the subsurface of the South Atlantic, offshore Brazil and West Africa, have led to more studies on travertines and lacustrine carbonates accumulated in continental rift basins (Abilio and Inkollu, 1989; Wright, 2012; Dorobek et al., 2012; Ronchi and Cruciani, 2015; Wright and Barnett, 2015). Despite extensive study, the present knowledge on continental carbonate facies, their precipitation processes and the extrinsic and intrinsic factors controlling their depositional architecture is still limited (cf. Wright, 2012; Della Porta, 2015). However, only few known fossil travertine deposits have been noted in the pre-Quaternary geological record. The Messinian mixed carbonate–terrigenous succession of the Albegna Basin (Southern Tuscany, Central Italy), of nearly 70-m thickness, has not been studied in detail, despite being a valuable example of the interaction between travertines and colluvial–alluvial terrigenous deposits in a kilometre-scale fault-controlled rift basin. This study assesses the lithofacies characteristics and architecture as well as the factors controlling the sedimentary evolution over time of a mixed travertine–terrigenous succession. Thus, interpretative geological models are provided, which could prove useful in comparable outcrop and subsurface rift systems.

2. Geological setting

2.1. Structural and stratigraphic framework of Southern Tuscany

The Neogene Albegna Basin (Fig. 1) developed on the Cenozoic Apennine fold-and-thrust belt from the Tortonian (Late Miocene) Age, when the inner northern part of the Apennine orogen was subjected to extensional tectonics, which was equivalent in time to the eastward migration of the thrust propagation (Patacca et al., 1990; Carmignani et al., 1994). Extensional structures were superimposed on the previous contractional structures (Pasquarè et al., 1983; Zanchi and Tozzi, 1987; Brogi et al., 2014). The Albegna Basin substrate includes the following pre-extension superimposed tectonic units (Kligfield, 1979 and references therein): 1) Ligurian and Sub-Ligurian Units, composed of remnants of the Jurassic oceanic crust and its Jurassic–Cretaceous sedimentary cover, as well as Cretaceous–Oligocene turbidites; 2) Tuscan Nappe, composed of non-metamorphic sedimentary succession including the Upper Triassic Anidrite di Burano/Calcare Cavernoso Formation and Cretaceous–Lower Miocene marine clastic deposits; and 3) the metamorphic Tuscan succession.

The Miocene extensional phase led to the development of hinterland basins separated by NW–SE-oriented transverse lineaments (Pascucci et al., 2007). During the Pliocene, structural depressions developed controlled by WSW–ENE-oriented tectonic lines (Zanchi and Tozzi, 1987; Pascucci et al., 2007; Cornamusini et al., 2011 and references therein), such as the Albegna Line (Fig. 1). These extensional basins were filled by upper Tortonian lacustrine clays and fluvial conglomerates (Unit T in Bossio et al., 2003–2004; cf. Fig. 2), overlain by brackish deposits that denoted an early Messinian marine transgression (Unit M1 in Bossio et al., 2003–2004). The following uplift of the Middle Tuscany Ridge during the late Messinian promoted the deposition of fluvio-lacustrine conglomerates and clays (M3 in Bossio et al., 2003–2004). In the study area, unit M3 is represented by the Poggio Capraio Formation, which unconformably overlies the Ligurian Unit (Fig. 3). The Albegna Basin was oriented SSW–NNE during the Pliocene when at least 200 m of marine claystone were deposited (Blue Clays; Unit-P1 in Bossio et al., 2003–2004; Figs. 1 and 2). The Late Pliocene to Holocene sedimentary history of the Albegna Basin was characterized by

tectonic uplift as well as glacio-eustasy and climate changes, with the deposition of various continental lacustrine to brackish successions (Units P2, P3 and Q1–Q3; cf. Bossio et al. 2003–2004 and Fig. 2) unconformably overlying the Lower Pliocene marine Blue Clays.

2.2. Distribution of travertine outcrops in Albegna Basin

The Albegna Basin includes several Neogene to Holocene thermogene travertine units, which are distributed along faults and fractures, are related to hydrothermal activity, and occur close to the Manciano, Montemerano, Saturnia and Marsiliana localities (Fig. 1c; Zanchi and Tozzi, 1987; Bosi et al., 1996; Barilaro et al., 2011, 2012; Ronchi and Cruciani, 2015). Bosi et al. (1996) distinguished five travertine units of different ages from the Messinian to the Holocene (Tr1–Tr5 in Fig. 2). These authors determined the relative ages of these units based on their stratigraphic positions, sedimentary and tectonic features and, for the youngest units, their occurrence with respect to three orders of Quaternary fluvial terraces developed in the Albegna River valley, labelled as A1, A2 and A3 (Fig. 2). Tr1 represents the Holocene travertine deposits at Bagni di Saturnia (Fig. 1), which developed on the youngest and lowest (25–80 m above sea level, a.s.l.) fluvial terrace A1 (Bosi et al., 1996). This active system is characterized by a water temperature of 37 °C and a pH of 6.3 (Minissale, 2004). Tr2 denotes the Middle–Upper Pleistocene travertines cropping out near the Montemerano and Manciano villages, which developed on the fluvial terrace A2, from 80 to 160 m a.s.l. (Bosi et al., 1996). The Middle Pleistocene Tr3 travertines, which crop out at the village of Saturnia, are older than the A3 fluvial terrace (from 100 to 190 m a.s.l.; Bosi et al., 1996). These three travertine units are untilted and characterized by sub-horizontal stratification. Tr4 refers to Pliocene travertine deposits close to the village of Semproniano, which developed above the Pliocene deposits (Bosi et al., 1996); this unit is also characterized by horizontal stratification, although the travertines show evidence of tectonic deformation (Bosi et al., 1996). Tr5 represents the Messinian travertine deposits that crop out close to the Marsiliana village, which

are the focus of this study. The Tr5 travertines overlie the Messinian deposits with a tilted appearance (dips 60–70°), and they are subjected to faults with a strike-slip component as the underlying Messinian strata (Bosi et al., 1996; Bossio et al., 2003–2004).

3. Methods

The investigated Messinian travertine unit and the associated terrigenous deposits crop out close to the Marsiliana village, particularly within an active and an abandoned quarry (Fig. 3). Satellite images were examined to document the extensions of the quarry and relative deposits using the published geological maps of the area (Pertusati et al., 2004; Cornamusini et al., 2011). Field data were obtained through macro-scale observations, 14 detailed stratigraphic logs and lithofacies mapping. Stratigraphic sections, with thickness varying from 2.5 to 61.5 m, were logged to characterize the different lithofacies types. Hundreds of samples of travertines and terrigenous deposits were collected from the field, which were then prepared to produce polished slabs and thin sections. Petrographic analyses of 98 thin sections provided information on the microfabric types. The porosity of each distinguished lithofacies was determined by the qualitative visualization of the pore space percentage per area at the scale of both hand samples (areas of nearly 25–50 cm^2) and thin sections (areas of nearly 2–4 cm^2), using the image analyses software ImageJ.

With the use of Open Gis software (Q-GIS) and three-dimensional (3D) modelling software (Move Midland Valley, 2012), a detailed geological map and a 3D model of the spatial distribution of the distinguished lithofacies association could be obtained.

The mineralogical composition of two carbonate samples was determined using an X-ray powder diffractometer Philips X'Pert MPD with a high-temperature chamber. Stable carbon and oxygen isotopes were measured in 53 calcite samples, from different facies types, outcrops and stratigraphic levels. Carbonate powders were extracted with a dental microdrill without mixing the carbonate components. Stable isotope analyses were conducted using a MAT253 mass spectrometer

with an automated carbonate preparation device (gas bench II) at the University of Bochum, Institute for Geology, Mineralogy and Geophysics stable isotope facility. Stable isotope results were calibrated to the V-PDB scale by the international standards CO-1 and CO-8. The analytical precision is better than 0.07‰ for $\delta^{13}C$ and 0.13‰ for $\delta^{18}O$.

4. Lithofacies character and spatial distribution

The studied Messinian travertine–terrigenous succession cropping out at the Marsiliana active quarry is nearly 70 m thick and 300 m wide (Figs. 3–5). The tectonically tilted sedimentary unit dips towards the NW, with inclinations varying from a few degrees (4°) up to 70°, in the westernmost part of the quarry. The identified inverse and normal faults have steeply inclined fault planes and limited displacement, hence resulting in negligible disturbance.

The logged stratigraphic succession (Fig. 5) includes travertine deposits, which dominate in the lower portion and are overlain by or interfinger with terrigenous detrital strata in the intermediate and upper portion of the succession. Nine travertine lithofacies (Table 1) were distinguished based on meso- to micro-scale fabric characteristic and stratal architecture. They were labelled according to the terminology proposed by Chafetz and Folk (1984), D'Argenio and Ferreri (1986), Guo and Riding (1998), Jones and Renaut (2010), Barilaro et al. (2012), Gandin and Capezzuoli (2014) and Della Porta (2015). In this study, the term 'boundstone' is used to denote travertine lithofacies formed by a rigid framework of precipitated clotted peloidal micrite, already lithified at the time of deposition (cf. Della Porta, 2015). The term 'cementstone' is used to represent crystalline sparitic textures (cf. Wright, 1992; Della Porta, 2015). Travertine lithofacies consisting of grainy deposits were classified using the terminology of Dunham (1962) and Embry and Klovan (1971) for carbonate depositional textures. Based on X-ray diffraction (XRD) analysis, the carbonate mineralogy was found to be calcite. The five terrigenous lithofacies distinguished include detrital breccias, siliciclastic sandstone and claystone, as summarized in Table 2.

4.1. Clotted peloidal micrite and microsparite boundstone to grainstone (facies F1)

4.1.1. Description

Ranging from grainstone to boundstone, facies F1 is composed of irregular to sub-rounded grains of clotted peloidal micrite welded together to form an irregular framework (facies F1a) or dendritic shapes (facies F1b; Fig. 6A). The layers of facies 1 are centimetre thick, often undulated and locally associated with centimetre-scale erosional surfaces. Clotted peloidal micrite dendrites (facies F1b) develop perpendicular to the stratification, displaying a branching pattern with rounded terminations. Microscopically, the boundstone texture consists of clotted peloidal micrite and microsparite with either an irregular framework (Fig. 6B) or branching dendrites (Fig. 6C). The minor components of this facies are elongated moulds of reeds, gastropods and ostracodes, which are often surrounded by coatings of clotted peloidal micrite that are a few microns thick. Calcite cements, which are widespread, include the following components: 1) local growth of an irregular pendant cement at the bottom of the clots; 2) prismatic cement with scalenohedral terminations; and 3) pores subsequently filled with limpid equant cement, with a crystal size varying from a few microns up to 300 µm. The primary porosity consists of a sub-millimetre-scale framework, interparticle voids and irregular voids up to 1 cm in size, which are denoted as fenestrae. The secondary porosity consists of irregular vugs, 100–500 µm in size.

4.1.2. Interpretation

Several authors have attributed the precipitation of clotted peloidal micrite in both marine and non-marine environments to microbial mat mediated via various organomineralic pathways of biologically induced and influenced mineralization (Krumbein, 1979; Reitner, 1993; Reitner et al.,

1995; Dupraz et al., 2009; Pedley et al., 2009; Pedley, 2014). In thermogene travertines, clotted peloidal micrite is deposited mainly in pond and flat low-energy depositional environments (Guo and Riding, 1998; Gandin and Capezzuoli, 2014; Della Porta, 2015 and references therein), which leads to dendrite morphologies, termed as 'bacterial shrubs' (Chafetz and Folk, 1984; Chafetz and Guidry, 1999). Chafetz and Folk (1984) suggested that the precipitation process is significantly influenced by microbial mats and that shrub growth is promoted by sulphide-oxidizing bacteria in H_2S-rich thermal water. Fouke et al. (2000) and Fouke (2011) largely documented the presence of various microbial communities thriving in thermogene travertine depositional systems. Gandin and Capezzuoli (2014) observed that shrub morphologies also develop on sub-vertical walls characterized by rapid evaporation of thin sheets of thermal water. In the studied Marsiliana system, dendritic shrub boundstone facies are not widespread, although they do occur occasionally on sub-horizontal to gently inclined surfaces, at places of inferred slow thermal water flow. Erosional surfaces are produced by subaerial exposure and meteoric weathering, suggesting that the thermal water flow must have been intermittent and/or have changed path over time, thus exposing the travertine deposits to meteoric alteration (cf. Chafetz and Folk, 1984; Guo and Riding, 1998; Özkul et al., 2002; Özkul et al., 2014). Rounded and fenestral porosities can be produced by the precipitation of carbonate around trapped gas bubbles, probably generated by microbial activity (Chafetz and Folk, 1984; Guo and Riding, 1998; Pentecost, 2005; Jones and Renaut, 2010). The primary porosity in the Marsiliana samples is filled by calcite cement including meteoric vadose pendant cement and prismatic scalenohedral to blocky cement precipitated by hydrothermal or meteoric phreatic groundwater (Török, 2003; Flügel, 2004; Palmer, 2007).

4.2. Raft floatstone/rudstone (facies F2)

4.2.1. Description

Rafts are elongated fragments (0.1–5 cm in width and hundreds of microns in thickness) of calcite blades, which form lenses of rudstone/floatstone (0.5–10 cm thick and tens of metres wide) deposited parallel to the depositional surfaces (Fig. 6D). Rafts often occur in association with skeletal grains (gastropods and ostracodes) or coated reed fragments, or isolated in clotted peloidal micrite grainstone (facies F1a). Microscopically, rafts consist of micritic and microsparitic films (Fig. 6E), which are coated by micrite envelopes followed by scalenohedral prismatic crystals. The interparticle pores in rudstone textures are filled by a mosaic of equant calcite (Fig. 6F). The secondary porosity is characterized by the formation of vugs, 0.2–2 cm in size.

4.2.2. Interpretation

Rafts develop on the surface of stagnant pools (Guo and Riding, 1998), where surface water degassing of CO_2 and evaporation increase carbonate saturation, in turn leading to the precipitation of calcite or aragonite as thin films on the water surface (Folk et al., 1985). Various mechanisms may cause the formation of raft rudstones. According to Jones (1989) and Taylor et al. (2004), rafts can break when crystals, preferentially growing under the lower surface of the raft, increase in density, causing rafts to sink to the bottom of the pool. Other causes for raft breakage are water agitation due to wind, rain and current and the pressure exerted by gas bubbles under the raft surface (Folk et al., 1985; Guo and Riding, 1998; Gandin and Capezzuoli, 2014). In the Marsiliana travertine succession, rafts are interpreted as indicators of temporary stagnant water conditions in ponds. Prismatic and equant blocky calcite cements in facies F2 are formed in the saturated zone beneath pool floors and/or in the meteoric phreatic zone (cf. Clarke and Bourke, 2011).

4.3. Sub-rounded radial coated grain grainstone/packstone (facies F3)

4.3.1. Description

This facies (Fig. 7A) forms horizontal lenses (15–20 cm in width and up to 6 cm in thickness), often being associated with clotted peloidal grainstone, raft rudstone and the skeletal remains of gastropods and ostracodes. The coated grains are composed of an irregular concentric radial coating around the peloidal nuclei (Fig. 7B), and are embedded in micrite, microsparite and sparite. In some cases, the radial coated grains are organized into fining-upward centimetre-thick beds, in turn separated by massive microsparite layers. The coated grain nuclei consist of peloids, gastropod or ostracode skeletal fragments (50–200 µm in size), surrounded by turbid lozenge-shaped or prismatic crystals of up to 700-µm length growing radially away from the nuclei (Fig. 7C–D). The interparticle porosity is usually occluded by scalenohedral and equant sparite. The secondary porosity is rare, characterized by irregular vugs up to 2 mm in size.

4.3.2. Interpretation

Similar sub-rounded radially arranged coated grains have been detected in various thermogene travertine depositional systems (Chafetz and Folk, 1984; Guo and Riding, 1998; Rainey and Jones, 2009; Della Porta, 2015). These grains, termed as ‘radial pisoids’ by Chafetz and Folk (1984), form in pools of terraced slopes and in horizontally bedded depressions with periodic turbulence (Chafetz and Folk, 1984; Guo and Riding, 1998). The growth of such sub-rounded coated grains is proposed to be influenced by both abiotic and biotic processes (Guo and Riding, 1994). Precipitation commences in low-energy conditions, followed by certain changes in environmental factors, such as the increase in water supply and energy, promoting the abiotic precipitation of calcium carbonate, for instance, when the grains are transported from one pool to another in terraced systems (Guo and Riding, 1998; Rainey and Jones, 2009). In the Marsiliana succession studied, this facies is localized in lenses, representing the accumulations of radial coated grains deposited in pools behind obstacles to the thermal water flow in a terraced slope system.

4.4. Coated gas bubble boundstone (facies F4)

4.4.1. Description

This facies consists of micrite that precipitates around rounded to elongated upward pore spaces, with sizes varying from several microns up to 4 cm (Fig. 7E). Layers of coated bubbles are associated with raft rudstone (facies F2), reed rudstone and boundstone (facies F7), which vertically alternate with laminated boundstone (facies F6). The micrite coatings (of 50–100-µm thickness) might be overlain by dendrites hundreds of microns in thickness or by irregular micrite crusts. These coatings are embedded in a framework of clotted peloidal micrite and microsparite, which provide a rigid boundstone texture (Fig. 7F). Scalenohedral prismatic calcite cement grows on both the inner and outer sides of the micritic hollows (Fig. 7G). In some cases, crystal terminations are draped by a thin (10-µm) red film of Fe and Mn oxides.

4.4.2. Interpretation

Gas bubbles can be preserved if they are trapped and coated by rapid precipitation of calcium carbonate (Chafetz and Folk, 1984; Guo and Riding, 1998; Jones and Renaut, 2010). Elongated bubble shapes are formed either by vertical gas escape or when more bubbles join in vertically stacked trains (Chafetz and Folk, 1984). Gas bubbles in hydrothermal vent settings may be produced by CO_2 degassing generated by turbulent water (Jones and Renaut, 2010), or they may be produced in low-energy pools by microbial activity through respiration and photosynthesis (Chafetz and Folk, 1984; Guo and Riding, 1998; Özkul et al., 2002; Pentecost, 2005; Jones and Renaut, 2010). Guido and Campbell (2011) described coated bubbles (termed as ‘foam texture’) in

association with channelized geometries in a terraced system. In the Marsiliana system, coated gas bubbles form layers under the low-energy conditions of flat ponds and pools of terraced systems.

4.5. Crystalline dendrite cementstone (facies F5)

4.5.1. Description

Crystalline dendrite cementstone consists of crusts (Fig. 8A) of vertically elongated branching calcite crystals that are adjacent to each other, varying in thickness from 2 up to 15 cm (Fig. 8B). Crystalline dendrite cementstone layers alternate with clotted peloidal micrite grainstone (facies F1a), laminated boundstone (facies F6) and coated gas bubble boundstone (facies F4).

Dendrites are composed of lozenge-shaped turbid crystals, of up to 100–200-µm length and 50–100-µm width, which run outward, often from a central elongate crystal acting as a stalk (Fig. 8C). Generally, the central stalk crystals are straight of 50–100-µm width, exhibiting uniform extinction under crossed polarizers. The dendrites are surrounded by cloudy microsparite and limpid equant microsparite to sparite. The horizontal laminae, which interrupt the vertical crystal growth, are composed of clotted peloidal micrite (Fig. 8D, E).

4.5.2. Interpretation

Thermogene travertine crystalline dendrites (Jones and Renaut, 1995) have also been termed as ‘feather crystals’ by Guo and Riding (1998) and Chafetz and Folk (1984) and as ‘crystal shrubs’ by Chafetz and Guidry (1999). The precipitation of crystalline dendrites is controlled by the concentration of Ca^{2+} ions in thermal water (Jones and Renaut, 1995; Rainey and Jones, 2009). This crystalline fabric is formed under the high-energy conditions of smooth slopes, terraced slopes, pool rims and cascades (Guo and Riding, 1998; Rainey and Jones, 2009; Özkul et al., 2014). The

thickness of crystalline dendrites is proportional to precipitation rates and thermal water flow velocity (Guo and Riding, 1998), whereas the growth lamination is attributed to periodic changes in water flow (Pentecost, 2005). The crystalline dendrites of the Marsiliana travertines are interpreted as deposited under the turbulent conditions on slopes and pool rims during high discharge of thermal water and high rates of degassing and evaporation.

4.6. Laminated boundstone (facies F6)

4.6.1. Description

Laminated boundstone consists of dense calcite with wavy laminae (Fig. 9A), up to 2 mm in thickness and up to a few metres in width (2–3 m). These laminae are characterized by undulated patterns (Fig. 9B) that develop convex-upward morphologies. The pores between the laminae are lens shaped and horizontally elongated, but more frequently the laminae are amalgamated with no interlaminar porosity. This facies occur laterally adjacent to reed rudstone (facies F7) and alternate with crystalline dendrite cementstone (facies F5). The laminae consist of structureless micrite and clotted peloidal micrite, associated with microsparite (Fig. 9C). Scalenohedral and blocky sparite cements fill the primary porosity (Fig. 9C).

4.6.2. Interpretation

Laminated travertine fabrics have been interpreted as being precipitated by microbially mediated processes (cf. Rainey and Jones, 2009; Gandin and Capezzuoli, 2014). Generally, laminated boundstone forms under low-energy conditions, such as pools and ponds in terraced slope systems (Gandin and Capezzuoli, 2014). However, laminated boundstone can also precipitate on steeply inclined slopes under conditions of reduced volumes of flowing water from the

hydrothermal vents (Rainey and Jones, 2009; Della Porta, 2015). In the Marsiliana travertines, the laminated boundstone facies occurs on inclined surfaces mostly alternating with centimetre-thick crystalline crust cementstone (facies F5). The replacement of crystalline dendrites by laminated boundstone on slopes suggests a change in the vent discharge rate, leading to a reduced output of thermal water.

4.7. Coated reed boundstone to rudstone/packstone (facies F7)

4.7.1. Description

Facies F7 is characterized by the presence of carbonate-encrusted plant stem moulds that appear as hollow tubes either vertically oriented perpendicular to the stratification or prostrated (Fig. 9D–E). Two types of facies F7 are identified. Reed boundstone (facies F7a) is composed of encrusted bushes of reeds that grew vertically and formed horizontal layers (5–20 cm thick), often above terrigenous deposits, extending laterally for up to 10 m. Phytoclastic rudstone/packstone (facies F7b) consists of prostrated and fragmented carbonate-coated reed stems deposited as sub-horizontal layers, in association with rafts, coated bubbles, mollusc skeletal remains and peloidal grainstone. Facies F7 is either associated with the F1–F4 travertine facies or it overlies terrigenous deposits (facies F10 to F14). The stem coating consists of homogeneous micrite, clotted peloidal micrite and microsparite, developing thin (10–20-µm) films, similar to the layers around the gas bubbles; reed moulds are rarely coated by lozenge-shaped crystalline dendrites. The inner wall of the micrite coating serves as the substrate for the growth of scalenohedral prismatic cement and equant calcite crystals (Fig. 9G).

4.7.2. Interpretation

The coated reed boundstone F7a represents in situ reed bushes encrusted by precipitated carbonate in life position, whereas F7b packstone/rudstone represents the reworking of fragments of carbonate coated vegetation. The presence of coated reeds, peloids and skeletal remains of ostracodes and gastropods suggests the reduced influence of thermal water, either cooled down in distal settings farther away from the vent or mixed with freshwater of ambient temperature, in marsh depositional environments (Guo and Riding, 1998; Özkul et al., 2002, 2014; Guido and Campbell, 2011; Capezzuoli et al., 2014). In the Marsiliana travertines, the occurrence of facies F7 overlying terrigenous deposits (F10–F14) is interpreted as indicators of depositional settings distal form the hydrothermal vent. Field observations of the active hydrothermal system (Bagni di Saturnia Holocene thermogene travertine in Fig. 1) show that vegetation colonizes the travertine surface after subaerial exposure or grows in dry areas adjacent to the active thermal water (with a temperature up to 37 °C) being the water flow temporarily deviated in other directions. In these instances, the plant stems are encrusted by the precipitation of calcium carbonate when a renewed flux of thermal water floods the substrate on which they grow. Hence, in the Marsiliana travertines, when facies F7 occurs in association with facies F1–F4, reeds probably grew on the lateral edges of pools where water did not temporarily flow.

4.8. Skeletal peloidal packstone/grainstone to floatstone/rudstone (facies F8)

4.8.1. Description

This lithotype consists of sub-horizontal nodular layers or concave-shaped lenses (5–60 cm thick) of skeletal peloidal packstone/grainstone to floatstone (Fig. 10A–B), with a grain size of 1–5 mm, rarely up to a few centimetres (Fig. 10C). Facies F8 is associated with clotted peloidal micrite grainstone (facies F1a) and reed facies (facies F7). Skeletal grains include gastropods, bivalves and ostracodes; they often appear as biomoulds coated by 1–2-mm-thick clotted peloidal micrite crusts

and filled by clots of peloidal micrite of 20–30-µm size. The non-skeletal grains include faecal pellets (Fig. 10D), and aggregates of clotted peloidal micrite. Equant sparite cement fills the interparticle and intraparticle pores (Fig. 10E–F). In the upper part of the studied stratigraphic succession, pendant cement occurs in discontinuous crusts.

4.8.2. Interpretation

Lithotypes rich in clotted peloidal micrite, skeletal remains and faecal pellets typically occur in low-energy environments as ponds and pools. The occurrence of common molluscs and ostracodes is indicative of fresher and/or cooler waters than those precipitating travertine facies F1–F6. This lithotype is not generally associated with thermogene travertine facies, but it could develop at the edges of travertine systems. Guo and Riding (1998) and Guido and Campbell (2011) identified similar facies, which were rich in skeletal fragments and clotted peloidal micrite, in marsh environments developed at the distal end of travertine slopes. According to Freytet and Verrecchia (2002), some of the micritic and microsparitic coatings around grains might have developed in the vadose zone. Armenteros et al. (1997) described a similar nodular appearance, attributing it to palustrine environments, transitional between lacustrine and alluvial plain deposits. In the Marsiliana succession, facies F8 can be interpreted as being deposited in shallow marshs and low-energy freshwater environments with possible fluctuations of the water level.

4.9. Calci-mudstone to microsparstone (facies F9)

4.9.1. Description

This lithotype occurs as a dense homogeneous grey or red carbonate precipitate, deposited in sub-horizontal layers of thickness ranging from 2–3 to rarely 10 cm. Facies F9 does not show any

sedimentary structure, and it alternates laterally and vertically with clotted peloidal grainstone (F1), raft (F2) and reed rudstone (F7) and coated gas bubble boundstone facies (F4). This calci-mudstone consists of aggregates of clotted peloidal micrite, structureless micrite and microsparite, gastropods, ostracodes and rafts (Fig. 10G–H). Blocky sparite cement has equant crystals sized 200–300 µm.

4.9.2. Interpretation

This massive facies is interpreted as accumulated in low-energy stagnant water pool settings, originating from sedimentation of carbonate mud derived from detrital, evaporative or biologically influenced processes. The microsparstone fabric may be derived from the diagenetic alteration of micrite or be primarily precipitated as micrite.

4.10. Breccia (facies F10)

4.10.1. Description

This facies consists of poorly sorted, matrix- to grain-supported breccias (Fig. 11A) with angular and subangular clasts (size ranging from several millimetres to 80 cm). The breccia layers (thickness varying from 1 m to >10 m; Fig. 5) are massive or crudely bedded in lobate or sheet-like geometry at a width of tens of metres, which decrease in thickness and pinch out towards the N–NW direction. Inverse and normal grading and erosional bases can be observed. The composition of the clasts includes >80% of dark-coloured, recrystallized calci-mudstone to microsparstone associated with fine-grained sandstone, siltstone, limestone, travertine reddened clasts and rare claystone lithic fragments. The interparticle space is filled by a detrital matrix consisting of structureless micrite and microsparite, as well as terrigenous silt and clays.

4.10.2. Interpretation

These breccia deposits are interpreted as gravity-flow fans, similar to those described by Leeder (2009), which developed along linear mountains front-fed by channels perpendicular to the axis of the main valley. Gravity flows are commonly observed in sedimentary basins bounded by thrust or normal faults, where periodic fault movements trigger slope instability and preserve the detrital fan deposits in the downthrown subsiding areas (cf. Leeder, 2009). Blikra and Nemec (1998) interpreted similar deposits in western Norway as high-viscosity debris flows in postglacial colluvial systems, which developed along the slopes of valley sides. In the studied succession, clast size, poor sorting and the uniform composition of the largely angular clasts suggest that the F10 breccias were deposited in a proximal colluvial fan system (cf. Blikra and Nemec, 1998). The main source of the carbonate clasts were the Ligurian and Tuscan Nappe Units (cf. paragraph 2.1 and Fig. 1), which crop out at the footwall of the fault system located south of the studied succession (Fig. 3). The micrite matrix among breccia clasts was likely to be derived from the abrasion and erosion of the carbonate clasts.

4.11. Conglomerate (facies F11)

4.11.1. Description

The facies F11 conglomerate consists of moderately sorted clasts, from subangular to rounded, mostly composed of dark-grey calci-mudstone (>80% of the clasts, ranging in size from a few millimetres to 20 cm; Fig. 11B). These conglomerates are often associated with sandstone facies (facies F12 and F13) in coarsening-upward sequences overlying the facies F14 claystone. They form lens-shaped, concave-upward layers (up to 50–60 cm in thickness) extending laterally from a few metres to hundreds of metres. The F11 conglomerate beds with erosional bases overlie

claystone (facies F14) in the eastern area and travertines toward the western area of the active quarry (Figs. 3, 4 and 5). Some conglomerate beds display clast imbrications, and inverse or normal grading. The carbonate matrix consists of both structureless micrite and clotted peloidal micrite and microsparite.

4.11.2. Interpretation

Zembo (2010) interpreted similar lithofacies in the Val d'Agri Quaternary continental succession (Southern Italy) as deposits of sheet floods or channelized gravelly streams that entered a low-energy environment, such as a marginal shallow lake. This interpretation can be applied to the Marsiliana F11 conglomerate. The source of the calci-mudstone clasts is interpreted to be the erosion of the tilted rocks of the Tuscan Nappe and the Ligurian Units substrate, as for the F10 breccias. The filling of the interparticle space by clotted peloidal micrite and microsparite probably occurred under subaquatic low-energy conditions in shallow ponds of an alluvial plain.

4.12. Massive sandstone (facies F12)

4.12.1. Description

These sandstones form 5–20-cm-thick tabular beds and lenses that extend laterally for 5–10 m, without any internal sedimentary structures, except for a weak lamination (Fig. 11C). Various grains (medium to coarse sand of 0.5–2-mm size) are embedded in a carbonate mud matrix: dark-coloured limestone clasts, quartz grains and rare micas. This facies is mainly associated with facies F10, and more rarely with facies F14 and F11 in fining- or coarsening-upward sequences up to 30 cm in thickness.

4.12.2. Interpretation

This massive sandstone lithofacies is interpreted as the finer portion of colluvial fan gravity-flow deposits, in association with the F10 breccia deposits. Miall (1996) described similar facies in sediment gravity-flow deposits, which they attributed to the progradation of colluvial fans when sandstones are overlain by breccias in coarsening-upward sequences (Blikra and Nemec, 1998). Massive F12 sandstones in coarsening-upward sequences between facies F14 at the base and the F11 conglomerate at the top are interpreted as accumulations under subaqueous low-energy conditions in shallow ponds of an alluvial plain, similar to the lithofacies interpreted by Zembo (2010).

4.13. Laminated sandstone to siltstone (facies F13)

4.13.1. Description

This facies is composed of fine sandstone to siltstone beds (5–20 cm thick, laterally extended for up to 30 m), yellow to grey in colour with normal gradation, and planar or undulate lamination (Fig. 11D). Sand grains are composed of lithic fragments of dark calci-mudstone and microsparstone, as well as siliciclastic siltstone, quartz and mica detrital grains. This facies is organized in both fining- and coarsening-upward trends when it overlies conglomerate (facies F11) and claystone beds (facies F14), respectively.

4.13.2. Interpretation

Laminated sandstone to siltstone facies are interpreted as deposits due to suspension and weak traction current in the overbank areas of an alluvial plain (Miall, 1996). When cross-laminated

sandstones are interbedded with claystones, they can be interpreted as being deposited in the shoreline facies of lakes and ponds in an alluvial plain (cf. Link et al., 1978), or in fluvial lower-flow-regime conditions (Miall, 1996). In the Marsiliana succession, when facies F13 is associated with travertines of facies F7, it is interpreted as deposits on the margins of shallow water ponds; instead, when it is associated with conglomerates (facies F11), it is interpreted as being deposited by weak traction currents of streams and settling from suspension in an alluvial plain.

4.14. Claystone (facies F14)

4.14.1. Description

These deposits consist of claystones, grey in colour, massive, and nodular or finely laminated, displaying root moulds and carbonate nodules belonging to palaeosols (Fig. 11E–F). The thickness varies from a few centimetres up to 1.70 m (maximum thickness in the eastern area), laterally extending from a few centimetres to a width of 20–30 m.

4.14.2. Interpretation

Miall (1996) interpreted similar deposits as accumulations in standing pools, backswamps, overbanks or abandoned channels or as drape deposits in alluvial settings. Massive claystones are interpreted as being settled from suspension, following flood events in the mudflat areas of alluvial environments (Miall, 1996). Neves et al. (2005) interpreted similar facies associated with gravel deposits and developed in lenses, in relation to the formation of ponds with settlement of fine sediment. In the Marsiliana succession, in association with the F11 conglomerate and the F13 laminated sandstone, this facies F14 is interpreted as being deposited in an alluvial plain, with the development of shallow ponds or in overbank areas subjected to subaerial exposure and

pedogenesis. In association with the F10 breccias, this claystone facies is interpreted as being deposited in standing water pools developed on the colluvial fan systems.

4.15. Oxygen and carbon stable isotope analyses

The Marsiliana travertines display $\delta^{18}O$ signatures varying from −10.5 to −6.1‰ V-PDB, and $\delta^{13}C$ values from −1.9 to 3.9‰ V-PDB (Fig. 12). The various types of travertine facies differ in their $\delta^{13}C$ values, which might reflect a different primary signature or the effect of meteoric diagenesis. Higher average $\delta^{13}C$ values are observed in F1 and F5 facies (1.7‰ and 1.9‰, respectively), whereas the lowest $\delta^{13}C$ average values are noted in facies F4 and F8 (−0.6‰ V-PDB and 0.3‰ V-PDB, respectively). The rest of the travertine facies can be subdivided into two classes based on the average of their $\delta^{13}C$ values, with F2 and F3 having a signature >1‰ and F7 and F9 <1‰. The average travertine $\delta^{18}O$ values vary between −8.1‰ (facies F7) and −7.1‰ (facies F5), which is of a narrower range than the $\delta^{13}C$ signatures. The $\delta^{18}O$ average values of facies F1, F8 and F9 are approximately −7.7‰. Instead, the F3 and F4 $\delta^{18}O$ values are −7.3‰ and −7.1‰, respectively. In the upper 20–25 m of the stratigraphic succession (Fig. 5), the $\delta^{13}C$ and $\delta^{18}O$ values of the travertines collected show decreasing trends from the bottom to the top (logs SA and F; Figs. 5 and 12) and from South to North.

5. Depositional environments and sedimentary evolution over time

5.1. Lithofacies association

The vertical stacking and lateral spatial distribution of the distinguished lithofacies types is shown in the correlation diagram of the measured stratigraphic logs in Fig. 5, as well as in the

lithofacies map and digital elevation model of Figs. 13 and 14. The lithofacies are assigned to four associations based on the interpretation of the depositional environment and their spatial distribution. The identified lithofacies associations are as follows: a) travertine slope (facies F1–F6), b) travertine flat (facies F1–F3 and F7–F9), c) alluvial plain (facies F11–14) and d) colluvial fan (facies F10, F12).

5.1.1. Travertine slope lithofacies association

The travertine slope lithofacies association comprises facies F1–F6, accumulated in terraced and smooth slope depositional settings that alternate laterally and vertically, just as Özkul et al. (2002) and Claes et al. (2015) described the Pamukkale travertines. According to Guo and Riding (1999), slope terraces form when the water rapidly flows in laminar sheets on gently dipping topographic surfaces, and raised rims and walls begin to deposit due to turbulence, evaporation and obstacles to the flow.

This lithofacies association occupies the lower 20 m of the studied succession (logs G, PB, MC, P in Fig. 5), mainly in the central and western part (Figs. 13 and 14), further interfingering with claystone and conglomerate layers in the eastern part (facies 11 and 14 in log N of Fig. 5). Moreover, travertine lenses, intercalated within the breccia deposits (facies F10) in log E, belong to the slope lithofacies association. The travertine slope environment must have been affected by intermittent thermal water flow, as suggested by the periodic exposure to meteoric alteration (Fig. 15A) and alternation with terrigenous breccia deposits.

The Marsiliana terraced slope lithofacies association is characterized by a layered (0.5–5-cm-thick beds) down-stepping morphology with sub-horizontal metre-scale pools separated by rounded rims and sub-vertical walls (Fig. 15B–C). The walls of the terraces vary in height from a few millimetres (micro-terraces; Fig. 15D) up to 1 m; the inclined walls and rims consist of clotted peloidal micrite grainstone to boundstone (facies F1) and 2–4-cm-thick crystalline dendrite

cementstone (facies F5) layers. Sub-horizontal layers form 3–4-m-wide pools, characterized by a concave-upward bottom of a depth of a few centimetres, and fronted by decimetre-thick rims on the downstream side, which is inferred to have been towards the NW direction based on the down-stepping topography (Fig. 15E–F). The pool lithofacies include raft rudstone (facies F2), radial coated grain grainstone (facies F3), coated gas bubble boundstone (facies F4) and reed rudstone to boundstone (facies F7). The pool travertines are characterized by a porous framework (Fig. 15E), due to the presence of intra-bubble and mouldic porosity. When the slope is smooth and inclined between 10° and 30° (logs P and PB in Fig. 5), it is composed of 10–15-cm-thick layers of crystalline dendrite cementstone (facies F5), alternating with 2–5-cm-thick layers of laminated boundstone (facies F6).

The geochemical signature of the travertine slope lithofacies association (average $\delta^{13}C$ 1.43 ‰ with a maximum of 3.88 ‰; average $\delta^{18}O$ of −7.50 ‰) confirms that the precipitating water was fed by geothermally generated CO_2, as reported in various studies on thermogene travertines (Pentecost, 2005; Capezzuoli and Gandin, 2008; Della Porta, 2015).

5.1.2. Travertine flat lithofacies association

This lithofacies association is characterized by tabular sub-horizontal beds varying in thickness from a few centimetres to 1–2 dm (Fig. 16A–B). It is dominated by reed rudstone to boundstone (facies F7), skeletal peloidal packstone/grainstone to floatstone/rudstone (facies F8) and calci-mudstone/microsparstone (facies F9) with rare clotted peloidal micrite boundstone to grainstone (facies F1), raft rudstone (facies F2) and radial coated grain grainstone (facies F3). The travertine flat lithofacies association is interpreted as shallow pond deposits under conditions of stagnant or slow-flowing thermal water that was likely to be mixed with meteoric water, according to the low $\delta^{13}C$ values. These conditions can occur either in distal areas with respect to the vent or in proximal areas, but only after events of subaerial exposures identified by the underlying

terrigenous deposits and the development of erosional surfaces and pedogenesis, or during terminal phases of the hydrothermal activity and thermogene travertine formation.

Travertine flat lithofacies types occur in stratigraphic logs G and CRA in the western part of the studied quarry (Figs. 5, 13 and 14), in the upper part of log D, in the entire expanse of log SA, in log MC and P in the central part of the quarry, at the top of logs F and in log N in the eastern part. In stratigraphic logs G, MC, P and N, the travertine flat lithofacies association is identified at the bottom of the studied succession, where it overlies the alluvial plain lithofacies association and is overlain by the travertine slope lithofacies association. By contrast, in the upper part of the studied area (stratigraphic logs CRA, D, SA and F in Fig. 5), the travertine flat did not evolve into the slope lithofacies association. The travertine flat lithofacies association characterizes the northern part of the studied area (Fig. 3), and it is noted in the stratigraphic log CE and MA as well (Fig. 16C–D), where it is 20 m thick (in 10–80-cm thick sub-horizontal beds) and extend laterally for a width of 50 m.

The average $\delta^{13}C$ value of the travertine flat is 0.46‰, varying from a minimum value of −1.9 ‰ to a maximum of 2.18 ‰. The lower (negative) $\delta^{13}C$ values (Fig. 12) were measured in samples from logs CRA, SA and F in the upper part of the succession, which show an inverse covariance with increasing $\delta^{18}O$ and decreasing $\delta^{13}C$ values. This trend of $\delta^{18}O$ is suggested to be indicative of soil-derived CO_2 and cooling of the travertine precipitating water likely due to mixing with meteoric water (Deocampo, 2010). According to Guo and Riding (1998) and Guido and Campbell (2011), distal travertine flat lithofacies should record the significant influence of meteoric freshwater. The highest (positive) values of $\delta^{13}C$ were recorded in samples from the travertine flat lithofacies cropping out in the northern abandoned quarry (Fig. 3), farther away from the southern faults and the supposed location of the vent. This increase in $\delta^{13}C$ might be attributed to the progressive degassing of CO_2 at increasing distances from the vent (Fouke et al., 2000; Kele et al., 2008; Faccenna et al., 2008; Della Porta, 2015).

5.1.3. Alluvial plain lithofacies association

This lithofacies association represents the lateral and vertical transitions of the terrigenous facies F11, F12, F13 and F14 (Fig. 17A) and the occurrence of travertines enriched in phytoclasts (facies F7) and skeletal fragments (facies F8), in the form of lenses of 1–2-dm thickness and 5–6-m width (Fig. 17B–C). These travertines are often associated with thick (80–120 cm) deposits of massive and laminated (facies F14) claystone (Fig. 17D, E). This lithofacies association is interpreted as being indicative of an alluvial plain (facies F14) with channelized streams (lenticular beds of facies F11–13), shallow marshes and palustrine ponds (facies F7, F8), cropping out mostly in the eastern and upper parts of the study area. The alluvial plain lithofacies are well developed in the following regions: a) in the eastern stratigraphic logs F and N; b) in the uppermost part of log D; c) in logs DM and DS, where they are interbedded with the breccia deposits (facies F10); and d) in logs P, MC and G (Fig. 17F), in the lower part of the studied quarry, where alluvial plain lithofacies occur between the travertine slope and the travertine flat lithofacies association.

5.1.4. Colluvial fan lithofacies association

This lithofacies association consists of 10–20-m-thick deposits of amalgamated breccia beds (facies F10) with erosional bases (Fig. 18A–D), alternating with decimetre-thick massive sandstone beds (facies F12) and rare, massive claystone of <1-m thickness (facies F14). Laterally, this lithofacies association extends for 100–200 m, with the breccia beds decreasing in thickness and pinching out northwards. This lithofacies association represents proximal debris flow-dominated colluvial fans (cf. Blikra and Nemec, 1998). Nemec and Kazanci (1999) described a similar lithofacies association in the Taurus Mountains, west-central Anatolia (Turkey), concluding that the development of such thick colluvial fans is characteristic of a semi-arid climate, where occasional rainstorms trigger debris flows. This interpretation may also be applied to the facies F10 breccias.

In addition, because the uplifted substrate sedimentary rocks may have been the source of the debris-flow clasts, a tectonic trigger for the generation of debris flow cannot be excluded in the Albegna extensional basin, as in other continental rift basins (cf. Heward, 1978).

The colluvial fan lithofacies association is recorded in stratigraphic logs CRA, E, P, D, DM and DS (Figs. 5, 13 and 14). In the eastern, lower part of the studied succession, the colluvial fan debris-flow deposits alternate with the alluvial plain lithofacies association (Fig. 18E). In the intermediate and upper portions (stratigraphic logs E and P), the colluvial fan deposits alternate with the travertine slope lithofacies association with seven alluvial fan units separated by six travertine lenses, forming layers of thickness ranging from a few centimetres up to 2–3 m (Fig. 16F). This shows that the thermal water flow was still active, promoting the rapid re-establishment of terraced travertine morphologies after the emplacement of the colluvial fans. In the upper part, colluvial fans interfinger with the alluvial plain lithofacies association (the top of stratigraphic log D; Fig. 5).

5.2. Stratigraphic architecture and evolution of the depositional system

Based on the lithofacies characteristics and association, spatial distribution, geometry and vertical and lateral lithofacies transitions, the studied sedimentary succession can be divided into three parts representing three different progressive phases, from older to younger, of evolution of the deposition in a tectonically controlled sedimentary basin (Figs. 13, 14, 19 and 20).

5.2.1. Phase I

Phase I is characterized by the deposition of nearly 20 m of thermogene travertines in the form of terraced and smooth slope aprons at the base of the studied succession (Figs. 14, 19 and 20A). Travertine slopes dip and thin towards the N and NW direction, indicating that the

hydrothermal vents might have been located close to the faults reported in the geological map at the southern border of the study area (Fig. 3). Hydrothermal vents are often linked to fault systems, as described by Sant'Anna et al. (2004) in the Itaboraí Basin (Brazil), and by Guido and Campbell (2011) in the Deseado Massif (Argentina), in the Rapolano Terme fissure ridge (Brogi and Capezzuoli, 2009) and in Della Porta (2015) in rift lakes from Western USA. An alluvial plain environment extended from the East towards the West and North adjacent to the growth of the travertine slope system (Fig. 20A). Similarly, Szulc et al. (2006) described alluvial deposits in association with travertines in the Upper Triassic of Southern Poland, as did Zentmyer et al. (2008) along the Holocene South Tibetan (China) fault system.

The accumulation of the travertine slope must have become an active component of the evolving landscape, thus obstructing the deposition of the alluvial plain environment, changing the direction of the superficial stream flow and promoting the formation of shallow ponds around the travertine deposits.

5.2.2. Phase II

Phase II (of nearly 30-m thickness) is marked by the onset and accumulation of tens of metres of colluvial fan breccias that buried the travertine slope system of Phase I. Colluvial fans thinned northwards and westwards (Fig. 20B), whereas this lithofacies association interfingered with the persistent alluvial plain environment in the eastern part of the studied succession. The occurrence of alluvial plain deposits in the western part of the quarry (Figs. 13 and 14) suggests that the alluvial plain environment surrounded the colluvial fans.

In the literature, Hernandez-Diaz and Hernandez-Enrile (2001) have already reported the precipitation of travertines related to colluvial debris-flow lobes. These authors described the accumulation of Pleistocene to Holocene travertine deposits in a pull-apart basin in the Betic Cordillera (Spain). Ten Veen et al. (2004) reported a similar lithofacies succession in the Eşen ay

Basin in SW Turkey, as did Zentmyer et al. (2008) near Nyalam in Tibet. Jones and Arzani (2005) described the superposition of debris-flow breccias and travertine lenses in the Plio-Pleistocene succession of the Khrud Mountain belt in Central Iran.

The deposition of the colluvial fans might have been triggered by fault displacements related to the Neogene extensional tectonics in Southern Tuscany (see paragraph 5.1.4). During Phase II, the hydrothermal system was active but travertines could accumulate only during periods of quiescence of debris-flow deposition. During these periods, the alluvial plain environment extended towards the West and the North.

5.2.3. Phase III

Phase III (20–25 m in thickness) includes the interfingering of travertine flat and alluvial plain lithofacies associations representing adjacent and time-equivalent depositional environments (Fig. 20C). Phase III does not present a record of the travertine slope and colluvial fan lithofacies association. These two lithofacies associations may be absent due to removal by erosion or more likely due to non-deposition, because the sedimentary basin evolved into a flat plain with alluvial terrigenous deposits, channelized streams, marshes with vegetation (alluvial plain lithofacies association) and travertine deposits that reflect the terminal phases of hydrothermal activity (travertine flat lithofacies association). The travertine flat lithofacies were deposited in shallow ponds fed by thermal water mixed with groundwater charged with meteoric carrier. This is supported by the low negative $\delta^{13}C$ stable isotope data of the flat travertine lithofacies association at the top of the studied succession.

This evolution of the sedimentary succession might indicate a phase of tectonic quiescence and reduced displacement of extensional faults, which resulted in reduced hydrothermal activity and lack of travertine slope development, reduced creation of accommodation space, and filling of the basin with alluvial plain deposits. The lack of a colluvial fan lithofacies association in Phase III

might be attributed to the reduced fault-controlled creation of structural highs, which acted as sources of coarse detrital sediment.

6. Discussion: Factors controlling the Messinian mixed travertine–terrigenous succession

The evolution of a sedimentary basin depends on extrinsic and intrinsic controlling factors that determine the deposition of different lithofacies types and their stratigraphic architecture. The studied Messinian fault-controlled basin contains vertical superposition and lateral transition between thermogene travertines and terrigenous deposits influenced by hydrothermal activity, tectonics and climate.

The lateral distribution of travertine facies in a thermogene system depends on the rates of water discharge out of the vent and the distance from the hydrothermal vent, due to the decrease in water temperature and the mixing with meteoric water away from the vent (Pentecost, 2005). This is reflected in travertine lithofacies associations that change from a proximal slope to a distal marsh flat, as described by Guo and Riding (1998) and Guido and Campbell (2011). In the Marsiliana succession, thermogene travertines are localized in the southern and older (lower) parts of the studied area, especially during Phase I when a travertine slope system evolved laterally into distal flat lithofacies. In the younger (upper) part, the influence of both thermal and meteoric water is recorded; during Phase III, travertines accumulated in the form of flat lithofacies association.

The deposition of travertines and geothermal systems are a common feature in Southern Tuscany during the Neogene–Holocene due to magmatism (Serri, 1997) and extensional tectonics (Patacca et al., 1990) that facilitated thermal activity and the influx of mantle CO_2 since the Tortonian Age (Minissale, 1991). As reported by Minissale (2004), a geothermal field in Central Italy led to the hydrolysis of carbonates and further generation of CO_2 via metamorphic decarbonation reactions of the buried Mesozoic marine limestone successions. CO_2 must have

dissolved the evaporite and carbonate rocks of the Anidrite di Burano/Calcare Cavernoso Formation, producing Ca_2^+ and HCO_3^- ions that saturated the groundwater under the Albegna Basin. According to Forti et al. (1990), Doveri and Mussi (2014) and Guastaldi et al. (2014), the Mesozoic carbonate formations constitute an important regional aquifer in Southern Tuscany that feeds the active hydrothermal springs in present day (Minissale et al., 2002b). In addition to the Marsiliana travertines, other Miocene thermogene deposits have been identified in the adjacent Ombrone Basin (Bossio et al., 2003–2004) and in the Volterra Basin, close to Pignano (Gandin et al., 2002; Capezzuoli et al., 2004, 2009).

Active tectonics is another important factor that controls sedimentation in continental settings, creating accommodation space for sediment accumulation through fault-controlled subsidence. The association between travertines and active tectonics is evident in rift and pull-apart basins, as documented in several studies, for instance, by Altunel and Hancock (1993), Hernandez-Diaz and Hernandez-Enrile (2001), Özkul et al. (2002), Sant'Anna et al. (2004), Zentmyer et al. (2008), Guido and Campbell (2011), Nishikawa et al. (2012) and Henchiri (2014). The presence of normal and oblique faults provides paths for groundwater flow, rock fracturing and permeability increase (Sibson, 1996). In association with a geothermal field and a carbonate aquifer, these features permit the generation of thermogene travertine systems that can aggrade or prograde based on the interplay between travertine precipitation rates (function of thermal water discharge) and fault-induced subsidence. Bettelli et al. (1992) and Pertusati et al. (2004) recognized normal faults, running in the E–W direction, located to the south of the Marsiliana travertine deposits (Fig. 3). The orientation of the faults (Fig. 3) and of the travertine slope environment of phases I and II that pinch out northwards (Figs. 13, 14 and 20a,b) indicates that the hydrothermal vents must have been located to the south of the studied quarry, close to the faults. These faults must have linked the surface with the aquifer that accommodated the hydrothermal groundwater. In addition, tectonic activity and fault-block uplift might have favoured the formation of gravity-flow fans, as reported in several studies (Heward, 1978; Blair, 1987; Neves et al., 2005; Leeder, 2009).

Climate is a fundamental controlling factor of basin hydrology with a consequent effect on spring-related travertines. Travertines precipitate in almost all climatic belts, but mostly in humid and warm climates, where high atmospheric precipitation rates recharge the groundwater circulation (Viles and Pentecost, 2007), although intensive rainfalls induce water dilution of calcium carbonate ions (Pentecost, 2005; Jones and Renaut, 2010). In arid climates, despite the reduced recharge of the aquifers, travertine precipitation may be favoured by higher evaporation rates and warmer waters (Guodie et al., 1993; Ford and Pedley, 1996; Evans, 1999; Jones and Renaut, 2010). At temperate latitudes such as Central Italy, alternating phases of thermogene travertine accretion/erosion have been linked to Pleistocene palaeoclimatic oscillations (Faccenna et al., 2008; De Filippis et al., 2013). Palynological data collected on Messinian deposits in the Piedmont and Emilia-Romagna regions (Bertini, 2006; Bertini and Martinetto, 2011) and in the Po valley (Fauquette et al., 2006) in Northern Italy reveal that palaeoclimatic conditions were warm and humid in these zones during the late Messinian, with precipitation ranging from 400 up to 1600 mm/year (Fauquette et al., 2006). Moreover, Fauquette et al. (2014) confirmed that vegetation in the Northern Apennines during the late Neogene and the early Pleistocene was similar to that observed in present-day subtropical South-East China, with travertine deposits of Tengchong occurring in the Yunnan province (Jones and Peng, 2012). This suggests that a hypothetical humid climate might have favoured the development of the late Messinian Marsiliana hydrothermal system and travertine deposition.

The three distinguished phases in the Marsiliana succession mark the evolution of a mixed travertine–terrigenous system controlled by tectonic activity and climate. The tectonics created accommodation space; linked the groundwater pathways with a geothermal heating source through faults; and triggered fault-block uplift, erosion and deposition of the colluvial fans. The climate controlled the basin hydrology, groundwater recharge and possibly the rates of travertine deposition.

7. Conclusions

The mixed Messinian terrigenous–carbonate succession, well exposed within an active quarry near the village of Marsiliana (Albegna Basin, Southern Tuscany, Central Italy), exhibits a wedge-shaped geometry thinning in the N–NW direction, which accumulated in an extensional basin controlled by faults located to the South. The stratigraphic evolution of the basin consists of three phases, distinguished based on the spatial and temporal distribution and depositional architecture of four lithofacies associations. Nine thermogene travertine lithofacies (F1–F9) compose the 1) terraced and smooth slopes and 2) travertine flat lithofacies associations. The terrigenous lithofacies associations consist of five lithofacies (F10–F14) and include the 3) alluvial plain and 4) colluvial fans depositional environments.

Phase I was characterized by the interplay between the travertine slope (facies F1–F7) thinning in the N–NW direction and the alluvial plain environment extending from the East towards the North and West. During Phase II, the accommodation space was filled by colluvial fans formed by stacked debris-flow breccias, reaching a thickness of nearly 30 m (facies F10 and F12), separated by events of metre-scale travertine precipitation. Phase III recorded a change in deposition with the accumulation of alluvial plain lithofacies including claystone, siltstone, sandstone and conglomerates (F11–14). During Phase III, the travertine lithofacies were indicative of shallow ponds and marsh environments with carbonate-coated reeds (F7–F9), with thermal water possibly mixing with meteoric groundwater, as confirmed by the decrease in carbon stable isotope data.

The evolution of the studied succession was influenced by external factors such as tectonics and climate. Active faulting controlled the creation of accommodation space for travertine and terrigenous sediment accumulation as well as the pathways of groundwater hydrothermal circulation to superficial vents; through fault-block uplift, it also promoted the sources of detrital sediment that fed the colluvial fan breccias. Climate might have played a role in the recharge of the

aquifer, thermal water discharge at the vents and consequently the precipitation rate of the travertine.

The continental mixed carbonate–terrigenous depositional system of Marsiliana represents a succession in an extensional basin at scale of tens of metres, providing valuable information about the interplay between thermogene travertine and alluvial/colluvial depositional environments and the controlling factors of lithofacies architecture through space and time. The depositional interpretations presented in detail might provide further insight into similar fault-controlled continental depositional systems.

Acknowledgements

The authors wish to thank Andrea Niedermayr (Ruhr-Universität, Bochum, Germany) for the oxygen and carbon stable isotope analysis and Curzio Maliverno (Milan University) for the preparation of thin sections. They also thank the IAS for providing the PGS grant to support PhD student fieldwork and lab analyses. The authors acknowledge Statoil, especially Giulio Casini and Klaas Verwer, for partly funding the project. They thank Bevilotti srl for permitting free access to the active quarry for collecting field data. They also wish to thank the editor Brian Jones and the reviewers Concha Arenas and Michal Gradzinski for their constructive comments, which have considerably improved the manuscript.

References

Abilio, S., Inkollu, S. N., 1989. Namibe basin: geology and hydrocarbon potential, Angola. AAPG Search and Discovery Article #91022©1989 AAPG Annual Convention, April 23-26, 1989, San Antonio, Texas.

Altunel, E., Hancock, P. L., 1993. Morphology and structural setting of Quaternary travertines at Pamukkale, Turkey. Geological Journal, 28(3-4), 335-346.

Altunel, E., Karabacak, V., 2005. Determination of horizontal extension from fissure-ridge travertines: a case study from the Denizli Basin, southwestern Turkey. Geodinamica Acta, 18(3-4), 333-342.

Armenteros, I., Daley, B., García, E., 1997. Lacustrine and palustrine facies in the Bembridge Limestone (late Eocene, Hampshire Basin) of the Isle of Wight, southern England. Palaeogeography, Palaeoclimatology, Palaeoecology, 128(1), 111-132.

Barilaro, F., Della Porta, G., Ripamonti, M., Capezzuoli, E., 2011. Petrographic and Facies Analysis of Pleistocene Travertines in Southern Tuscany, Central Italy. AAPG Search and Discovery Article #90124 © 2011 AAPG Annual Convention and Exhibition, April 10-13, 2011, Houston, Texas

Barilaro, F., Della Porta, G., Cappezuoli, E., 2012. Depositional geometry and fabric types of hydrothermal travertine deposits (Albegna Valley, Tuscany, Italy). Rend. Soc. Geol. Ital., 21, 1024–1025.

Beglinger, S. E., Doust, H., Cloetingh, S., 2012. Relating petroleum system and play development to basin evolution: West African South Atlantic basins. Marine and Petroleum Geology, 30(1), 1-25.

Bertini, A., 2006. The Northern Apennines palynological record as a contribute for the reconstruction of the Messinian palaeoenvironments. Sedimentary Geology, 188, 235-258.

Bertini, A., Martinetto, E., 2011. Reconstruction of vegetation transects for the Messinian–Piacenzian of Italy by means of comparative analysis of pollen, leaf and carpological records. Palaeogeography, Palaeoclimatology, Palaeoecology, 304(3), 230-246.

Bettelli, G., Bonazzi, U., Fazzini, P., Pellegrini, M., Fontana, D., Gasperi, G. F., 1992. Note alla Carta geologica del bacino del fiume Albegna. Bollettino della Società Geologica, 61(2).

Blair, T. C., 1987. Tectonic and hydrologic controls on cyclic alluvial fan, fluvial, and lacustrine rift-basin sedimentation, Jurassic-lowermost Cretaceous Todos Santos Formation, Chiapas, Mexico. Journal of Sedimentary Research, 57(5), 845-862.

Blikra, L. H., Nemec, W., 1998. Postglacial colluvium in western Norway: depositional processes, faces and paleoclimatic record. Sedimentology, 45, 909-959.

Bortolotti V., Fazzuoli M., Pandeli E., Principi G., Babbini A., Corti S., 2001. Geology of the central and eastern Elba Island, Italy. Ofioliti, 26(2a), 97–150.

Bosi C., Messina P., Rosati M., Sposato A., 1996. Età dei travertini della Toscana meridionale e relative implicazioni neotettoniche. Memorie Società Geologica Italiana, 51, 293-304.

Bossio, A., Foresi, L. M., Mazzei, R., Salvatorini, G., Sandrelli, F., Bilotti, M., Colli, A., Rossetto, R., 2003-2004. Geology and stratigraphy of the southern sector of the Neogene Albegna River basin (Grosseto, Tuscany, Italy). Geologia Romana, 37, 165-173.

Brogi, A., Capezzuoli, E., 2009. Travertine deposition and faulting: the fault-related travertine fissure-ridge at Terme S. Giovanni, Rapolano Terme (Italy). International Journal of Earth Sciences, 98(4), 931-947.

Brogi, A., Capezzuoli, E., Aqué, R., Branca, M., Voltaggio, M., 2010. Studying travertines for neotectonics investigations: Middle–Late Pleistocene syn-tectonic travertine deposition at Serre di Rapolano (Northern Apennines, Italy). International Journal of Earth Sciences, 99(6), 1383-1398.

Brogi, A., Liotta, D., Ruggieri, G., Capezzuoli, E., Meccheri, M., Dini, A., 2015. An overview on the characteristics of geothermal carbonate reservoirs in southern Tuscany. Italian Journal of Geosciences, doi: 10.3301/IJG.2014.41

Capezzuoli, E., Gandin, A., Sandrelli, F., 2004. Neogene-Quaternary continental carbonates: the Quaternary deposits of Valdelsa and the Miocene travertines of Pignano (Volterra). In: Morin, D., Bruni, P. (Eds.), The “Regione Toscana” project of geological mapping. Case histories and data acquisition. Regione Toscana. Press, Firenze, Italy, 89-96.

Capezzuoli, E., Gandin, A., Pedley, H. M., 2009, September. Travertine and calcareous tufa in Tuscany (Central Italy). In: Pascucci, V., Andreucci, S. (Eds.), 27th IAS Meeting of Sedimentology, Alghero, Italy. Fieldtrip Guidebook. Press, Alghero, Italy, 129-158.

Capezzuoli, E., Gandin, A., Pedley, M., 2014. Decoding tufa and travertine (fresh water carbonates) in the sedimentary record: The state of the art. Sedimentology, 61(1), 1-21.

Carmignani, L., Decandia, F. A., Fantozzi, P. L., Lazzarotto, A., Lotta, D., Meccherini, M., 1994. Tertiary extensional tectonics in Tuscany (Northern Apennines, Italy). Tectonophysics, 238, 295– 315.

Chafetz, H. S., Folk, R. L., 1984. Travertines: depositional morphology and the bacterially constructed constituents. Journal of Sedimentary Research, 54(1), 289-316.

Chafetz, H. S., Guidry, S. A., 1999. Bacterial shrubs, crystal shrubs, and ray-crystal shrubs: bacterial vs. abiotic precipitation. Sedimentary Geology, 126(1), 57-74.

Claes, H., Soete, J., Noten, K., El Desouky, H., Marques Erthal, M., Vanhaecke, F., Özkul, M., Swennen, R., 2015. Sedimentology, three-dimensional geobody reconstruction and carbon dioxide origin of Pleistocene travertine deposits in the Ballık area (south-west Turkey). Sedimentology. Accepted Article; doi: 10.1111/sed.12188.

Clarke, J. D. A., Bourke, M. C., 2011. Travertine and tufa from Dalhousie Springs (Australia). Implications for recognizing Martian springs. Geological Society of America Special Papers, 483, 231-247.

Cornamusini, G., Foresi, L. M., Massa, G., Bonciani, F., Callegari, I., Da Prato, S., Ielpi, A., 2011. The Miocene successions of the Fiora Hills: considerations about the development of the minor basins of Southern Tuscany. Italian Journal of Geosciences, 130(3), 404-424.

D'Argenio, B., Ferreri, V., 1986. A brief outline of sedimentary models for Pleistocene travertine accumulation in southern Italy. Rendiconti Società Geologica Italiana, 9, 167-170.

Della Porta, G. 2015. Carbonate build-ups in lacustrine, hydrothermal and fluvial settings: comparing depositional geometry, fabric types and geochemical signature In: Bosence, D.

W. J., Gibbons, K. A., Le Heron, D. P., Morgan, W. A., Pritchard, T. & Vining, B. A. (eds), Microbial Carbonates in Space and Time: Implications for Global Exploration and Production. Geological Society, London, Special Publications, 418, 17-68.

Deocampo, D.M., Cuadros, J., Wing-Dudek, T., Olives, J., Amouric, M., 2009.

Saline lake diagenesis as revealed by coupled mineralogy and geochemistry of multiple ultrafine clay phases: Pliocene Olduvai Gorge, Tanzania. American Journal of Science 309, 834–868.

De Filippis, L., Faccenna, C., Billi, A., Anzalone, E., Brilli, M.,

Soligo, M., Tuccimei, P., 2013. Plateau versus fissure ridge travertines from Quaternary geothermal springs of Italy and Turkey: Interactions and feedbacks between fluid discharge, paleoclimate, and tectonics. Earth-Science Reviews 123 (2013) 35–52.

Dorobek, S., Piccoli, L., Coffey, B., Adams, A., 2012, Carbonate Rock-Forming Processes in the Pre-salt "Sag" Successions of Campos Basin, Offshore Brazil: Evidence for Seasonal, Dominantly Abiotic Carbonate Precipitation, Substrate Controls, and Broader Geologic Implications. AAPG Search and Discovery Article #90153©2012 AAPG Hedberg Conference Microbial Carbonate Reservoir Characterization, Houston, Texas, 3-8 June 2012

Doveri, M., Mussi, M., 2014. Water Isotopes as Environmental Tracers for Conceptual Understanding of Groundwater Flow: An Application for Fractured Aquifer Systems in the "Scansano-Magliano in Toscana" Area (Southern Tuscany, Italy). Water, 6(8), 2255-2277.

Dupraz, C., Reid, R. P., Braissant, O., Decho, A. W., Norman, R. S., Visscher, P. T., 2009. Processes of carbonate precipitation in modern microbial mats. Earth-Science Reviews, 96(3), 141-162.

Evans, J. E., 1999. Recognition and implications of Eocene tufas and travertines in the Chadron formation, White River Group, Badlands of South Dakota. Sedimentology, 46(5), 771-789.

Faccenna, C., Soligo, M., Billi, A., De Filippis, L., Funiciello, R., Rossetti, C., Tuccimei, P., 2008. Late Pleistocene depositional cycles of the Lapis Tiburtinus travertine (Tivoli, Central Italy):

possible influence of climate and fault activity. Global and Planetary Change, 63(4), 299-308.

Fauquette, S., Suc, J. P., Bertini, A., Popescu, S. M., Warny, S., Bachiri Taoufiq, N., Perez Villa, M. J., Chikhi, H., Feddi, N., Subally, D., Clauzon, G., Ferrier, J., 2006. How much did climate force the Messinian salinity crisis? Quantified climatic conditions from pollen records in the Mediterranean region. Palaeogeography, Palaeoclimatology, Palaeoecology, 238(1), 281-301.

Fauquette, S., Bertini, A., Manzi, V., Roveri, M., Argnani, A., Menichetti, E., 2014. Reconstruction of the Northern and Central Apennines (Italy) palaeoaltitudes during the late Neogene from pollen data. Review of Palaeobotany and Palynology, 218, 117-126.

Fazzuoli M., Pandeli E., Sani F., 1994. Considerations on the sedimentary and structural evolution of the Tuscan Domain since Early Liassic to Tortonian. Memorie Società Geologica Italiana 48, 31–50.

Folk R.L., Chafetz H.S., Tiezzi P.A., 1985. Bizarre forms of depositional and diagenetic calcite in hot-spring travertines, Central Italy. In: Schneidermann N., Harris P. (Eds.), Carbonate cements, Society of Economic Paleontologists and Mineralogists Special Publication, 36, 349–369.

Ford, T. D., & Pedley, H. M., 1996. A review of tufa and travertine deposits of the world. Earth-Science Reviews, 41(3), 117-175.

Fouke, B. W., 2011. Hot-spring Systems Geobiology: abiotic and biotic influences on travertine formation at Mammoth Hot Springs, Yellowstone National Park, USA. Sedimentology, 58(1), 170-219.

Fouke, B. W., Farmer, J. D., Des Marais, D. J., Pratt, L., Sturchio, N. C., Burns, P. C., Discipulo, M. K., 2000. Depositional facies and aqueous-solid geochemistry of travertine-depositing hot springs (Angel Terrace, Mammoth Hot Springs, Yellowstone National Park, USA). Journal of Sedimentary Research, 70(3), 565-585.

Flügel, E., 2004. Microfacies of carbonate rocks: analysis, interpretation and application. Springer Science & Business Media Berlin, 976 p..

Freytet, P., Verrecchia, E. P., 2002. Lacustrine and palustrine carbonate petrography: an overview. Journal of Paleolimnology, 27(2), 221-237.

Forti, P., Micheli, L., Piccini, L., Pranzini, G., 1990. The karst aquifers of Tuscany (Italy). In: Hydrogeological Processes in Karst Terrants (Proceedings of the Antaîya Symposium and Field Seminar, IAHS Publication, 207, 341-349.

Gandin, A., Capezzuoli E., Sandrelli F., 2002. A Messinian hot-spring travertine system and its system and its modern analogue at Rapolano in Southern Tuscany, Italy. 16th IAS Congress, Johannesburg, Abstract Volume, 110.

Gandin, A., Capezzuoli, E., 2008. Travertine versus calcareous tufa: distinctive petrologic features and stable isotopes signatures. Italian Journal of Quaternary Sciences, 21, 125-136.

Gandin, A., Capezzuoli, E., 2014. Travertine: Distinctive depositional fabrics of carbonates from thermal spring systems. Sedimentology, 61(1), 264-290.

Goudie, A. S., Viles, H. A., Pentecost, A., 1993. The late-Holocene tufa decline in Europe. The Holocene, 3(2), 181-186.

Guastaldi, E., Graziano, L., Liali, G., Brogna, F. N. A., Barbagli, A., 2014. Intrinsic vulnerability assessment of Saturnia thermal aquifer by means of three parametric methods: SINTACS, GODS and COP. Environmental Earth Sciences, 72, 2861–2878.

Guido, D. M., Campbell, K. A., 2011. Jurassic hot spring deposits of the Deseado Massif (Patagonia, Argentina): characteristics and controls on regional distribution. Journal of Volcanology and Geothermal Research, 203(1), 35-47.

Guo, L., Riding, R., 1994. Origin and diagenesis of Quaternary travertine shrub fabrics, Rapolano Terme, central Italy. Sedimentology, 41(3), 499-520.

Guo, L., Riding, R., 1998. Hot-spring travertine facies and sequences, Late Pleistocene, Rapolano Terme, Italy. Sedimentology, 45(1), 163-180.

Guo, L., Riding, R., 1999. Rapid facies changes in Holocene fissure ridge hot spring travertines, Rapolano Terme, Italy. Sedimentology, 46(6), 1145-1158.

Hancock, P. L., Chalmers, R. M. L., Altunel, E., Cakir, Z., 1999. Travitonics: using travertines in active fault studies. Journal of Structural Geology, 21(8), 903-916.

Henchiri, M., 2014. Sedimentology of Quaternary calcareous tufas from Gafsa, southwestern Tunisia. Arabian Journal of Geosciences, 7(5), 2081-2091.

Hernández-Díaz, J. M., Hernández-Enrile, J. L., 2001. Using travertine deformations to characterize paleoseismic activity along an active oblique-slip fault: the Alhama de Murcia fault (Betic Cordillera, Spain). Acta geológica hispánica, 36(3), 297-313.

Heward, A. P., 1978. Alluvial fan and lacustrine sediments from the Stephanian A and B (La Magdalena, Cinera Matallana and Sabero) coalfields, Northern Spain. Sedimentology, 25(4), 451-488.

Jones, B., Renaut, R. W., 1995. Noncrystallographic calcite dendrites from hot-spring deposits at Lake Bogoria, Kenya. Journal of Sedimentary Research, 65(1), 154-169.

Jones, B., 1989. Calcite rafts, peloids and micrite in cave deposits from Cayman Brac, British West Indies. Canadian Journal of Earth Sciences, 26, 654-664.

Jones, B., Renaut, R. W., 2010. Calcareous spring deposits in continental settings. Developments in Sedimentology, 61, 177-224.

Jones, B., Peng, X., 2012. Intrinsic versus extrinsic controls on the development of calcite dendrite bushes, Shuzhishi Spring, Rehai geothermal area, Tengchong, Yunnan Province, China. Sedimentary Geology, 249, 45-62.

Jones, S. J., Arzani, A., 2005. Alluvial fan response times to tectonic and climatic driven processes: example from the Khrud mountain belt, Central Iran. Geophysical Research Abstracts,7.

Kele, S., Demény, A., Siklósy, Z., Németh, T., Tóth, M., Kovács, M. B., 2008. Chemical and stable isotope composition of recent hot-water travertines and associated thermal waters, from

Egerszalók, Hungary: Depositional facies and non-equilibrium fractionation. Sedimentary Geology, 211(3), 53-72.

Kele, S., Özkul, M., Fórizs, I., Gökgöz, A., Baykara, M. O., Alçiçek, M. C., Németh, T., 2011. Stable isotope geochemical study of Pamukkale travertines: new evidences of low-temperature non-equilibrium calcite-water fractionation. Sedimentary Geology, 238(1), 191-212.

Kligfield, R., 1979. The Northern Apennines as a collisional orogen. American Journal of Science, 279(6), 676-691.

Krumbein, W. E., 1979. Calcification by Bacteria and Algae. Studies in Environmental Science, 3, 47-68.

Leeder, M. R., 2009. Sedimentology and sedimentary basins: from turbulence to tectonics. John Wiley & Sons, New York, USA, 592.

Link, M. H., Osborne, R. H., Awramik, S. M., 1978. Lacustrine stromatolites and associated sediments of the Pliocene ridge Route Formation, Ridge Basin, California. Journal of Sedimentary Research, 48(1), 143-158.

McCall, J., 2010. Lake Bogoria, Kenya: hot and warm springs, geysers and Holocene stromatolites. Earth-Science Reviews, 103(1), 71-79.

Miall, A. D., 1996. The Geology of Fluvial Deposits. Springer Verlag, Berlín, 582.

Minissale, A., 1991. Thermal springs in Italy: their relation to recent tectonics. Applied geochemistry, 6(2), 201-212.

Minissale, A., 2004. Origin, transport and discharge of CO_2 in central Italy. Earth-Science Reviews, 66(1), 89-141.

Minissale, A., Evans, W. C., Magro, G., Vaselli, O., 1997a. Multiple source components in gas manifestations from north-central Italy. Chemical Geology, 142(3), 175-192.

Minissale, A., Magro, G., Vaselli, O., Verrucchi, C., Perticone, I., 1997b. Geochemistry of water and gas discharges from the Mt. Amiata silicic complex and surrounding areas (central Italy). Journal of Volcanology and Geothermal research, 79(3), 223-251.

Minissale, A., Kerrick, D. M., Magro, G., Murrell, M. T., Paladini, M., Rihs, S., Sturchio, N.C., Tassi, F., Vaselli, O., 2002a. Geochemistry of Quaternary travertines in the region north of Rome (Italy): structural, hydrologic and paleoclimatic implications. Earth and Planetary Science Letters, 203(2), 709-728.

Minissale, A., Vaselli, O., Tassi, F., Magro, G., Grechi, G. P., 2002b. Fluid mixing in carbonate aquifers near Rapolano (central Italy): chemical and isotopic constraints. Applied geochemistry, 17(10), 1329-1342.

Nemec, W., Kazanci, N., 1999. Quaternary colluvium in west-central Anatolia: sedimentary facies and palaeoclimatic significance. Sedimentology, 46(1), 139-170.

Neves, M. A., Morales, N., Saad, A. R., 2005. Facies analysis of Tertiary alluvial fan deposits in the Jundiaí region, São Paulo, southeastern Brazil. Journal of South American Earth Sciences, 19(4), 513-524.

Nishikawa, O., Furuhashi, K., Masuyama, M., Ogata, T., Shiraishi, T., Shen, C. C., 2012. Radiocarbon dating of residual organic matter in travertine formed along the Yumoto Fault in Oga Peninsula, northeast Japan: implications for long-term hot spring activity under the influence of earthquakes. Sedimentary Geology, 243, 181-190.

Özkul, M., Varol, B., Alçiçek, M. C., 2002. Depositional environments and petrography of Denizli travertines. Bulletin of the Mineral Research and Exploration, 125, 13-29.

Özkul, M., Gökgöz, A., Kele, S., Baykara, M. O., Shen, C. C., Chang, Y. W., Kaya, A., Hançer, M., Aratman, C., Akin, T., Örü, Z., 2014. Sedimentological and geochemical characteristics of a fluvial travertine: A case from the eastern Mediterranean region. Sedimentology, 61(1), 291-318.

Palmer, A., N., 2007. Cave Geology. Dayton, Ohio. 454 p.

Pascucci, V., Martini, I. P., Sagri, M., Sandrelli, F., 2007. Effects of transverse structural lineaments on the Neogene–Quaternary basins of Tuscany (inner Northern Apennines, Italy). In: Nichols, G., Williams, E., Paola, C. (Eds.) Sedimentary Processes, Environments and Basins: A Tribute to Peter Friend, IAS Special Publication 38, 155-182.

Pasquarè, G., Chiesa, S., Vezzoli, L. and Zanchi, A., 1983. Evoluzione paleogeografica e strutturale di parte della Toscana meridionale a partire dal Miocene superiore. Memorie Società Geologica Italiana, 25, 145-157.

Patacca, E., Sartori, R., Scandone, P., 1990. Tyrrhenian basin and Apenninic arcs: Kinematic relations since Late Tortonian times, Memorie Società Geologica Italiana, 45, 425 – 451.

Pedley, H. M., 1990. Classification and environmental models of cool freshwater tufas. Sedimentary Geology, 68(1), 143-154.

Pedley, M., 2014. The morphology and function of thrombolitic calcite precipitating biofilms: A universal model derived from freshwater mesocosm experiments. Sedimentology, 61(1), 22-40.

Pedley, M., Rogerson, M., Middleton, R., 2009. Freshwater calcite precipitates from in vitro mesocosm flume experiments: a case for biomediation of tufas. Sedimentology, 56(2), 511-527.

Pentecost, A., 2005. Travertine. Springer Science & Business Media, Berlin, 445 p.

Pentecost, A., Viles, H., 1994. A review and reassessment of travertine classification. Géographie physique et Quaternaire, 48(3), 305-314.

Pertusati. P. C., Musumeci, G., Bonini, L. and Trumpy, E. (2004). Carta Geologica della Toscana, 1:10000, sezione 343050-Manciano.

Rainey, D. K., Jones, B., 2009. Abiotic versus biotic controls on the development of the Fairmont Hot Springs carbonate deposit, British Columbia, Canada. Sedimentology, 56(6), 1832-1857.

Reitner, D. D. J., 1993. Modern cryptic microbialite/metazoan facies from Lizard Island (Great Barrier Reef, Australia) formation and concepts. Facies, 29(1), 3-39.

Reitner, J., Neuweiler, F., Gautret, P., 1995. Modern and fossil automicrites: implications for mud mound genesis. In: Reitner, J. & Neuweiler, F. (coord.) A Polygenetic Spectrum of Fine-Grained Carbonate Buildups. Facies, 32, 4–17.

Ronchi, P., Cruciani, F., 2015. Continental carbonates as hydrocarbon reservoir, an analogue case study from the travertine of Saturnia, Italy. AAPG Bulletin, 99,711-734.

Sant'Anna, L. G., Riccomini, C., Rodrigues-Francisco, B. H., Sial, A. N., Carvalho, M. D., Moura, C. A. V., 2004. The Paleocene travertine system of the Itaboraí basin, Southeastern Brazil. Journal of South American Earth Sciences, 18(1), 11-25.

Serri, G., 1997. Neogene-Quaternary magmatic activity and its geodynamic implications in the Central Mediterranean region. Annals of Geophysics, 40(3).

Sibson, R. H., 1996. Structural permeability of fluid-driven fault-fracture meshes. Journal of Structural Geology, 18(8), 1031-1042.

Stein, M., 2001. The sedimentary and geochemical record of Neogene-Quaternary water bodies in the Dead Sea Basin-inferences for the regional paleoclimatic history. Journal of Paleolimnology, 26(3), 271-282.

Szulc, J., Gradzinski, M., Lewandowska, A., Heunisch, C., 2006. The Upper Triassic crenogenic limestones in Upper Silesia (southern Poland) and their paleoenvironmental context: In: Alonso-Zarza, A.M., Tanner, L.H. (Eds), Paleoenvironmental Record and Applications of Calcretes and palustrine Carbonates. Geological Society of America, Special Paper 416, 153-168.

Taylor, M. P., Drysdale, R. N., Carthew, K. D., 2004. The formation and environmental significance of calcite rafts in tropical tufa-depositing rivers of northern Australia. Sedimentology, 51(5), 1089-1101.

Ten Veen, J. H., Woodside, J. M., Zitter, T. A., Dumont, J. F., Mascle, J., & Volkonskaia, A., 2004. Neotectonic evolution of the Anaximander Mountains at the junction of the Hellenic and Cyprus arcs. Tectonophysics, 391(1), 35-65.

Török, Á., 2003. Facies analysis and genetic interpretation of travertine, Buda Vár-hegy, Hungary. Acta Geologica Hungarica, 46(2), 177-193.

Viles, H., Pentecost, A., 2007. Tufa and travertine. In: Nash, D., McLaren S. (Eds.) Geochemical Sediments and Landscapes, Blackwell, Oxford, 173-199.

Wright, V. P., 2012. Lacustrine carbonates in rift settings: the interaction of volcanic and microbial processes on carbonate deposition. In: Garland, J., Neilson, J. E., Laubach, S. E., Whidden, K. J. (Eds) Advances in Carbonate Exploration and Reservoir Analysis. Geological Society, London, Special Publications, 370, 39–47.

Wright, V. P., Barnett, A. J. 2015. An abiotic model for the development of textures in some South Atlantic early Cretaceous lacustrine carbonates. In: Bosence, D. W. J., Gibbons, K., Le Heron, D. P., Pritchard, T., Vining, B. (Eds) Microbial Carbonates in Space and Time: Implications for Global Exploration and Production. Geological Society, London, Special Publications, 418, 209-219.

Zanchi, A., Tozzi, M., 1987. Evoluzione paleogeografica e strutturale recente del bacino del fiume Albegna (Toscana meridionale). Geologica Romana, 26, 305-325.

Zembo, I., 2010. Stratigraphic architecture and quaternary evolution of the Val d'Agri intermontane basin (Southern Apennines, Italy). Sedimentary Geology, 223(3), 206-234.

Zentmyer, R., Myrow, P. M., Newell, D. L., 2008. Travertine deposits from along the South Tibetan fault system near Nyalam, Tibet. Geological Magazine, 145(06), 753-765.

Figure captions

Figure 1. Regional geological setting of the study area. A) The studied area is located in the Northern Apennines, in the Tuscany region, highlighted in orange. B) From Google Earth, satellite image of Tuscany, Central Italy, highlighted in orange; the Albegna Basin is framed in a black square. C) Geological map of the Albegna Basin redrafted after Cornamusini et al. (2011). From the Pliocene, the Albegna Basin is controlled by tectonic lineaments oriented SSW–NNE, such as the Albegna Line. The studied area is delimited by the black square.

Figure 2. Stratigraphy of the Neogene to the Holocene succession cropping out in the Albegna Basin, redrafted after the studies by Bosi et al. (1996) and Bossio et al. (2003–2004).

Figure 3. A) Geological map of the studied area redrafted after Pertusati et al. (2004). B) North–South geological cross section of the studied area showing the relationships of the Neogene M3 Unit Poggio Capraio Fm. with the deformed Mesozoic Anidrite di Burano/Calcare Cavernoso Formation and the Ligurian Unit.

Figure 4. Panoramic view of the exposed succession in the active quarry indicated in Fig. 3, which shows the location of the measured stratigraphic logs.

Figure 5. A) Correlation diagram of the measured stratigraphic logs. Green lines represent lithofacies correlation stratal surfaces tracked on the outcrop. Samples drilled for stable isotope analysis are reported on the right side of the stratigraphic logs (e.g., G02–G10.3 in log G). B) The legend of Fig. 5A shows the lithofacies grouped into lithofacies associations.

Figure 6. Polished slabs and photomicrographs of facies F1 (A–C), F2 (D–F) and F3 (D). A) Alternation of layers of clotted peloidal micrite grainstone (facies F1a) with undulated shape and clotted peloidal micrite boundstone (facies F1b), composed of pale-white micritic dendrites of up to 2-cm thickness. Dendrites develop centimetre-scale micro-terraces (red arrows). B) Facies F1a grainstone to boundstone consists of irregular clots, 200–500 µm in size, composed of peloidal micrite with 10–20-µm peloids; equant microsparite is seen between the clots. C) Photomicrograph of micritic branching dendrites (facies 1b) built by aggregates of peloidal micrite, growing perpendicular to the substratum. D) Polished slab of raft floatstone/rudstone (facies F2) made of

elongated calcite fragments surrounded by a white calcite coating. The primary interparticle porosity is widespread, but it is often filled by calcite cement. In the upper part of the slab, rafts are associated with sub-rounded radial coated grains, belonging to facies F3. E) Thin section showing rafts composed of recrystallized microsparite and enveloped by micrite coatings. F) Rafts are coated by different layers: from the base to top, the first layer consists of micrite followed by thin bladed cement (mic+bl), whereas the second layer consists of prismatic cement with scalenohedral termination up to 600 µm in thickness (pr), overlain by a mosaic of equant sparite (mo).

Figure 7. Outcrop photos, polished slabs and photomicrographs of facies F3 (A–D) and F4 (E–G). A) Sub-rounded radial coated grain grainstone (facies F3) deposited in sub-horizontal strata or concave lenses of 5-cm thickness, composed of white, millimetre-sized grains. B) Slab shows that coated grains have an irregular rounded shape, with a small dark core surrounded by white calcite coatings. The layers often occur in fining-upward sequences followed by massive microsparite-rich layers. C) The nuclei of sub-rounded radial coated grains can be composed of clots of micrite or microsparite and faecal pellets. The pores consist of irregular vugs of sizes up to 1–2 mm. D) The coating consists of radial lozenge calcite crystals with length up to 700 µm that grow adjacent to each other. Between the grains, calcite cement is composed of equant microsparite and sparite mosaics. E) Coated bubble boundstone (facies F4) consists of sub-rounded or vertically elongated hollows. The size of the hollows varies from a few millimetres up to 8 mm when the shape is vertically elongated. F) The thin section shows that the bubble coating is formed by micrite, constituting the substrate for the nucleation of micritic dendrites or undulated laminae that consist of peloidal micrite. G) Within the hollow, the growth of calcite cement is common, often comprising prismatic sparite with scalenohedral terminations.

Figure 8. Outcrop photos, polished slabs and photomicrographs of facies F5. A) The colour of crystalline dendrites varies from white to pink and yellowish. The vertical growth is often interrupted by horizontal undulated laminae made of millimetre-thick dendrites and dense travertine calci-mudstone (black arrow). B) Outcrop photo of crystalline dendrites, size of centimetres (up to 5

cm), growing vertically, perpendicular to the substrate. C) Crystalline dendrites consist of millimetre- to centimetre-long, branching composite crystals composed of lozenge-shaped turbid crystals (up to 100–200 µm long and 50 µm wide) running outwards with axial divergences of 10–30°. D) The thin section shows that the sub-horizontal lamination consists of alternations between thin crystalline calcite and clotted peloidal micrite (black arrow). E) Close-up view of crystalline dendrites crossed by sub-parallel micritic growth laminae.

Figure 9. Outcrop photos, polished slabs and photomicrographs of facies F6 and F7. A) Laminated boundstone consists of up to 5-cm-thick layers of wavy calcite laminae (2–5 mm thick), developing centimetre-thick terraces (black lines). B) Laminae consist of microsparite and clotted peloidal and structureless micrite. The cavities between the laminae are partially filled by equant sparite or are subjected to dissolution, thus developing irregular vugs up to 5 mm in size. C) Laminate boundstone composed of dense micrite laminae nearly 20 µm in thickness associated with clotted peloidal micrite. Primary interlaminar porosity is lined by scalenohedral cement. D) Example of vertical patches of reed moulds (facies F7a) >5 cm in height. On the right, prostrated and fragmented coated reed moulds (3–4 mm in diameter; facies F7b). E) Reed boundstone (facies F7a) consists of patches of sub-vertical or prostrate, centimetres-long carbonate-coated reed moulds. F) Photomicrograph of facies F7b phytoclastic packstone. G) Within the carbonate coating of reed moulds, the growth of prismatic sparite crystals with scalenohedral termination of up to 800-µm thickness is commonly observed.

Figure 10. Outcrop photos, polished slabs and photomicrographs of facies F8 and F9. A) Facies F8, in 5–10-cm-thick layers, consists of skeletal and peloidal packstone/grainstone to floatstone/rudstone. The skeletal components include gastropods, bivalves and ostracodes. B) Gastropod packstone/rudstone (facies F8) in sub-horizontal layers. C) Gastropods (Ga), up to 1 cm in size, are associated with millimetre-size faecal pellets (FP) and aggregates of clotted peloidal micrite (CPM). D) Photomicrograph of peloidal grainstone/packstone with faecal pellets up to 500 µm in size. E) Facies F8 peloidal grainstone with equant sparite cement. F) Photomicrograph of

gastropod peloidal grainstone with intraparticle porosity completely filled by sparite cement and clots of micrite. Around the large vug in the centre, scalenohedral calcite cement is observed. G). Facies F9 photomicrograph showing irregular aggregates of micrite and microsparite with vug porosity filled by equant calcite cement. H) The same image of panel 10G in crossed polarizers.

Figure 11. Outcrop photos and polished slabs of facies F10–F14. A) Breccias (facies F10) are made of dark-grey calci-mudstone to microsparstone clasts, from angular to subangular, with a micrite to microsparite matrix. Other components include clasts of cream sandstones, light-grey limestone and red travertine. B) Conglomerates (facies F11) consist of rounded to subangular clasts, with sizes ranging from sub-millimetres to centimetres, of recrystallized calci-mudstone and microsparstone; the interparticle spaces are filled by carbonate and terrigenous mud and mosaics of equant sparite (Eq). C) Massive sandstone (facies F12) consists of well-sorted, medium to coarse sand, with black calci-mudstone lithoclasts. D) Fine laminated sandstone to siltstone (facies F13) showing wavy lamination. E) Claystone (facies F14) is characterized by millimetre-thick lamination. F) Nodular claystone facies interpreted as pedogenetic features.

Figure 12. Stable isotope analyses of the Marsiliana studied succession with $\delta^{18}O$ and $\delta^{13}C$ values of the travertine samples distinguished based on lithofacies type and travertine lithofacies association, expressed in ‰ relative to the V-PDB scale: travertine slope lithofacies association is denoted in blue and travertine flat lithofacies association in green.

Figure 13. Map of the studied quarry showing the distribution of the four distinguished lithofacies associations, the three distinguished stratigraphic phases and the location of the stratigraphic logs.

Figure 14. A) 3D representation of the distribution of the lithofacies association draped on the digital elevation model of the studied area developed with the software Move Midland Valley. B) Panoramic view of the Marsiliana quarry superimposing the lithofacies association distribution and the location of the stratigraphic logs within the active quarry.

Figure 15. Outcrop photos of travertine slope lithofacies association. A) Convex-upward pool rim of nearly 45-cm thickness indicated by the black lines, covered by centimetre-thick yellow claystone, highlighted by the red lines. B) Terraced slope pool rim adjacent to sub-horizontal pools. The travertine is dark brown in colour due to exposure to meteoric weathering (exp). C) Terraces show a semicircular shape in plain view; the rim and wall lithofacies are white in colour, whereas the pool deposits are darker in colour, due to the concentrations of terrigenous detrital sediment. D) Centimetre-size micro-terraces that grow above a sub-horizontal surface. E) Detail of porous coated gas bubble boundstone decimetre-thick layers accumulated in a pool of the terraced slope. F) At the toe of the wall, the pool layers are characterized by a concave geometry, which becomes sub-horizontal when the pool is filled by carbonate precipitates.

Figure 16. Outcrop photos of travertine flat lithofacies association. A) Centimetre- to decimetre-thick beds of travertine flat lithofacies association (TR) overlain by breccia (Br; facies F10) in the lower part of log CRA. B) Travertine flat lithofacies association at the top of stratigraphic log F characterized by vertical coated reeds (arrow) and mouldic and fenestral millimetre-size porosity. C) Panoramic view of the northern part of the studied area, with travertine strata from the flat environment dipping towards the NW direction due to tectonic tilting. D) Outcrop photo of stratigraphic log CE, with travertine flat sub-parallel layers white and grey in colour.

Figure 17. Outcrop photos of alluvial plain lithofacies association. A) Alluvial plain lithofacies association in the lower eastern part of the studied area consisting of facies F11, F13 and F14, deposited in layers of thickness varying from centimetres to 1 m, alternating with travertines slope facies association (Tr). B) Travertine lenses (Tr) that are brown to slightly reddish in colour are intercalated in decimetre-thick claystone deposits. The occurrence of imbricate pebbles (IMB) confirms the deposition of F11 conglomerates in flowing water with traction. C) Close-up view of travertine layered phytoclastic- and skeletal-rich deposits (Tr; facies F7 and F8) that develop 20-cm-thick undulated lenses. D) Lens of claystone (facies F14) deposited between laminated

sandstone (facies F13) and the conglomerate (facies F11). E) Claystone layer of 6-cm thickness (facies F14) interpreted as overbank deposit in the alluvial plain, overlain by 10–20-cm-thick breccia (facies F10) and 10-cm-thick massive sandstone (facies F12) of the colluvial fan lithofacies association. F) Alluvial plain lithofacies in stratigraphic log G including conglomerate facies (F11) with clasts of up to 1-dm size.

Figure 18. Outcrop photos of colluvial fan debris flow and alluvial plain lithofacies associations. A) Colluvial fan debris-flow lithofacies association occurs in 10–20-m-thick breccia deposits with an erosional base (black line). B) Detail of breccia erosional base overlying travertine strata (black line). C) Colluvial fan debris-flow breccia overlying in sharp contact the travertine slope lithofacies. D) Detail of the sharp contact between the travertine slope comprising crystalline crusts (facies F5) and the overlying breccia bed. E) Colluvial fan breccia (F10) with intercalations of sandstone and siltstone (F12 and F13; black lines). F) Thermogene travertine lenses belonging to facies F1 (black arrows), thickness ranging from centimetres to metres and width from metres to decametres, in-between the colluvial fan breccias.

Figure 19. Correlation diagram of the measured stratigraphic logs showing the vertical and lateral distribution of the four distinguished lithofacies associations during the three phases of stratigraphic evolution. Legend in Fig. 20.

Figure 20. A) A possible paleoenvironmental reconstruction of Phase I, representing a travertine slope system evolving distally into a travertine flat, ultimately obstructing the deposition of the adjacent alluvial plain environment. 1) Alluvial plain consists of 1–2-m-thick strata of claystone (facies F14) with decimetre-thick channelized conglomerate (facies F11) and sandstone (facies F13). 2) Travertine terraces consist of sub-horizontal pools (facies F1–F4), pool rims and walls (facies F5). B) Interpretative model of Phase II with colluvial fan debris flow-dominated facies association overlain by travertine slope wedges. Laterally, towards the East, the alluvial plain environment overlies the travertine and colluvial fan lithofacies 3) Breccia (facies F10) with a thickness of several metres and massive sandstone deposits (facies F12) with thickness ranging

from centimetres to decimetres form the colluvial fan. C) A possible paleoenvironmental reconstruction of Phase III in which the travertine system evolved into a travertine flat characterized by freshwater marshy environments. 4) In the eastern part, Phase III consists of claystone terrigenous deposits, lenses of conglomerates (facies F11) and travertine marshes. Towards the NW, the travertine flat deposits interfinger with alluvial plain laminated sandstones to siltstones and claystones (facies F13 and F14). D) Legend for Fig. 19 and 20 facies and lithofacies associations.

Table 1. Description and environmental interpretation of the travertine lithofacies identified in the studied succession.

Table 2. Description and environmental interpretation of the siliciclastic lithofacies identified in the studied succession.

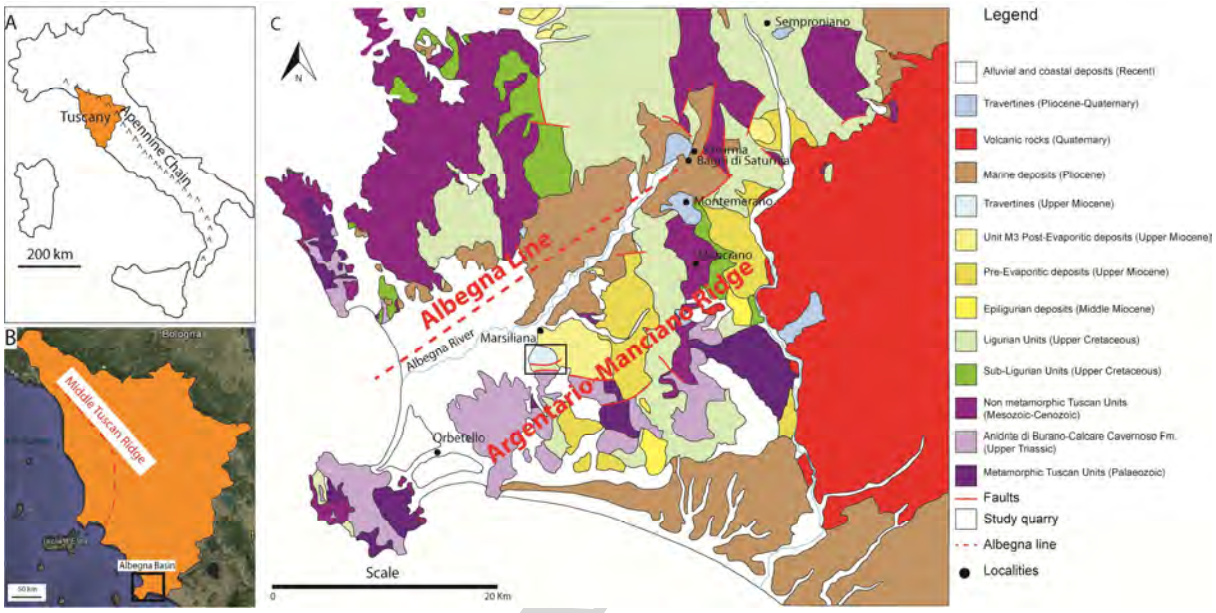

Figure 1

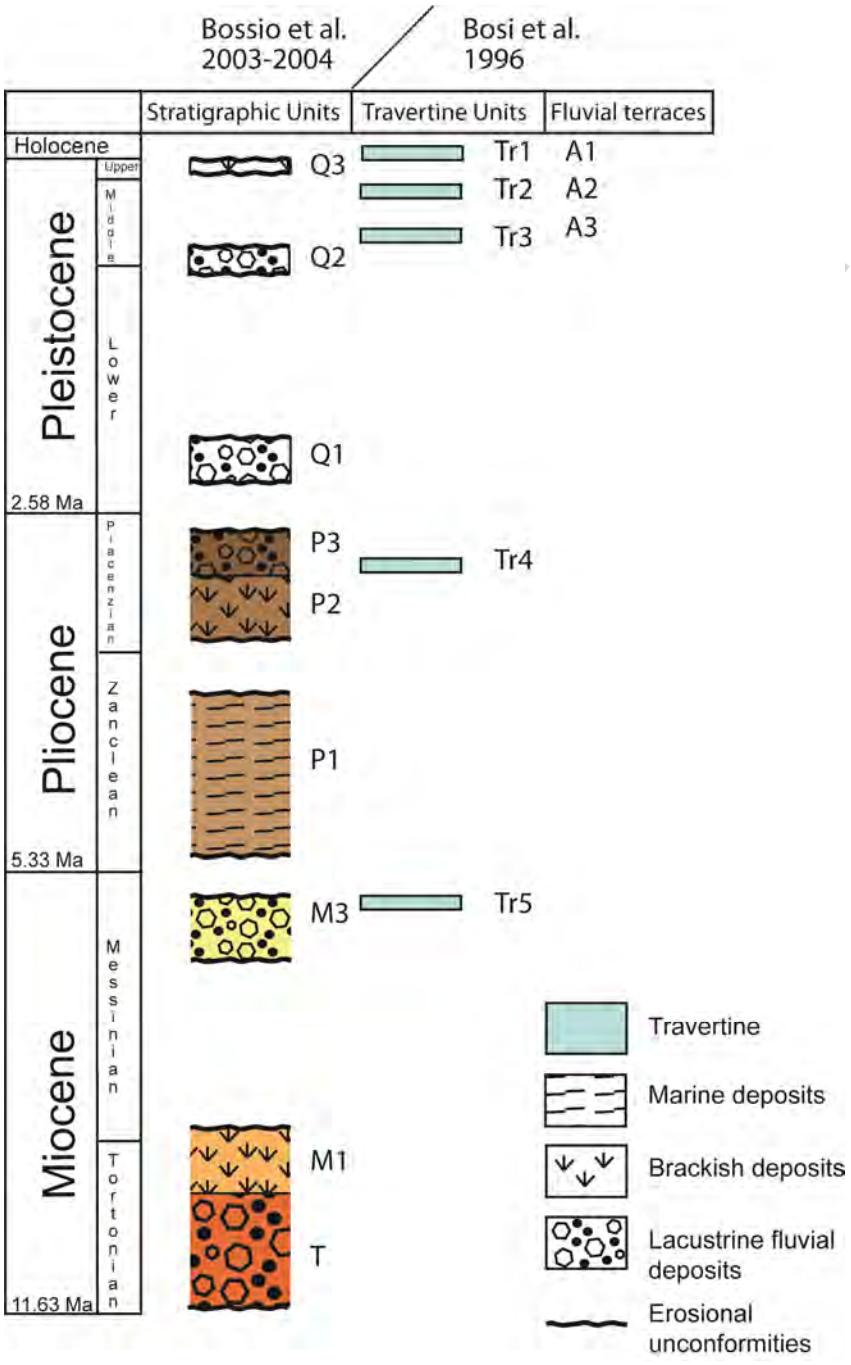

Figure 2

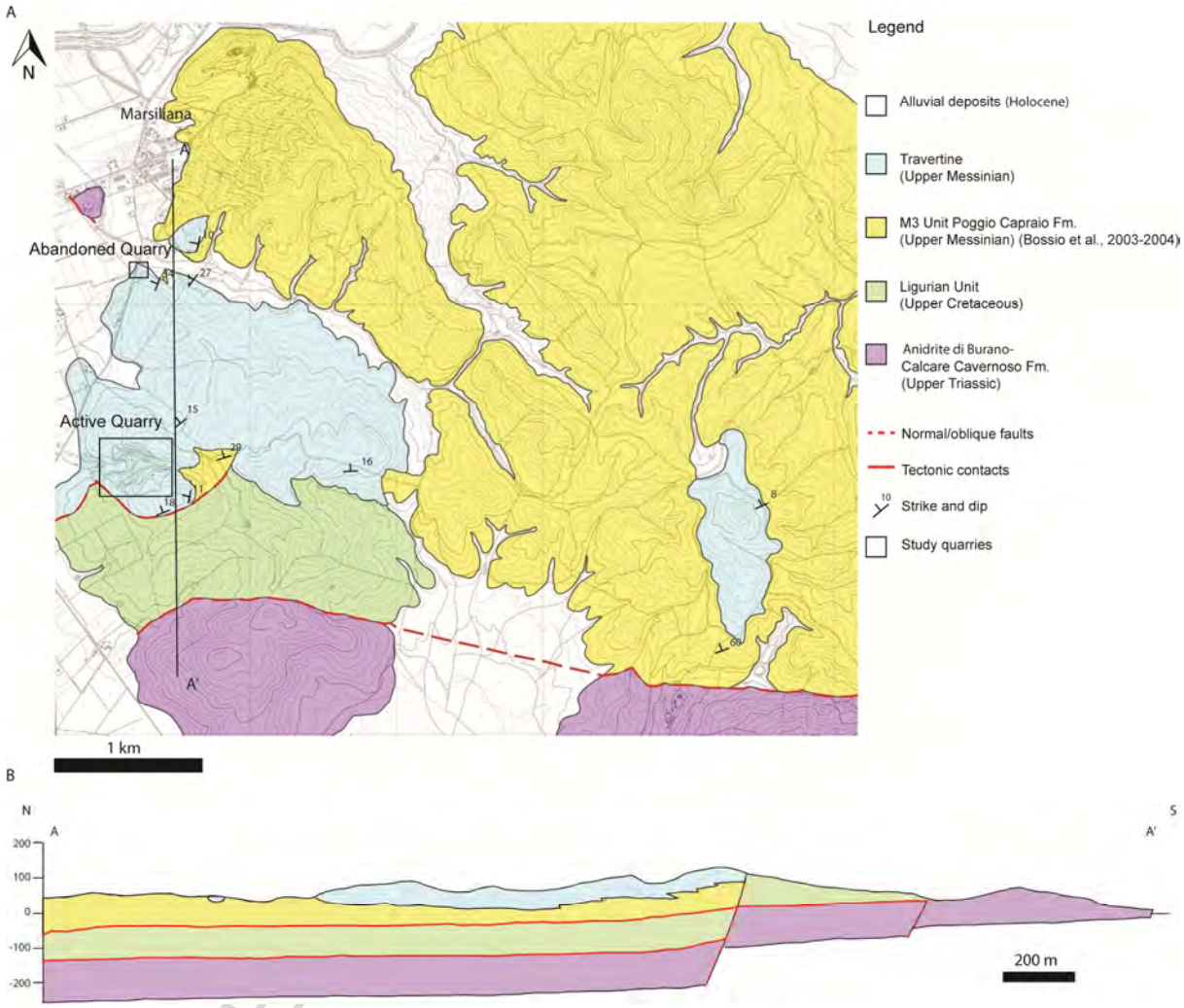

Figure 3

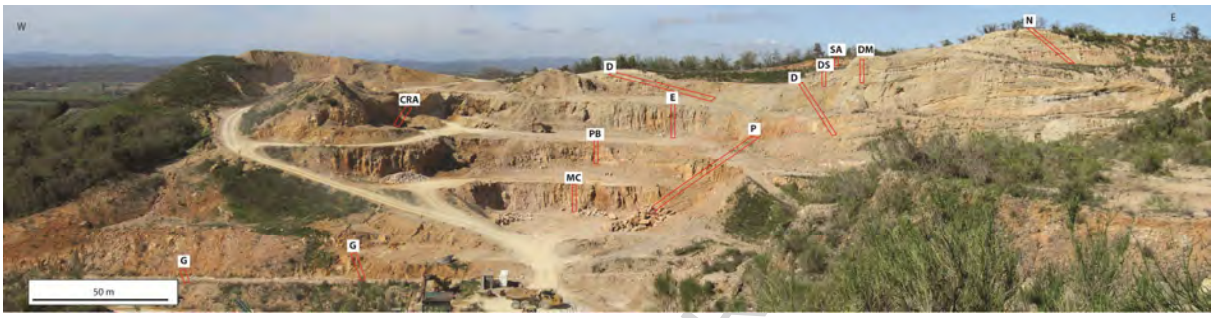

Figure 4

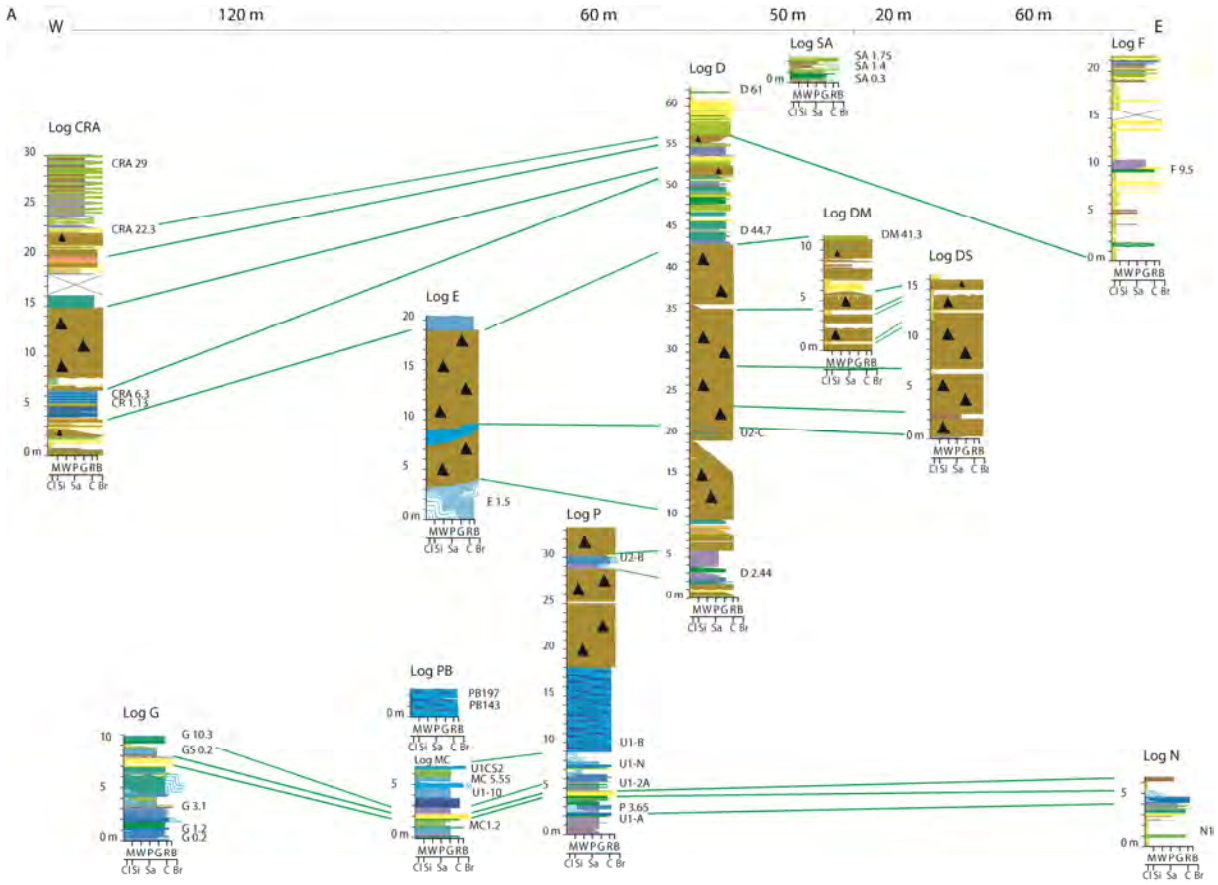

Figure 5a

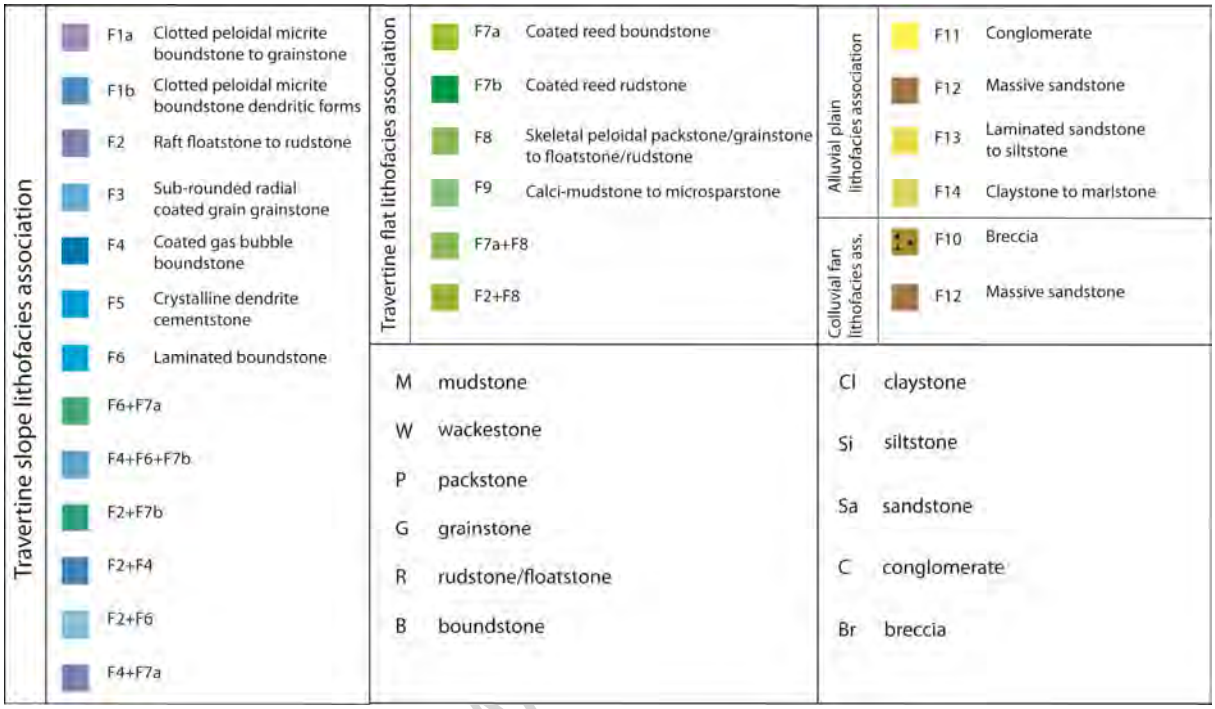

Figure 5b

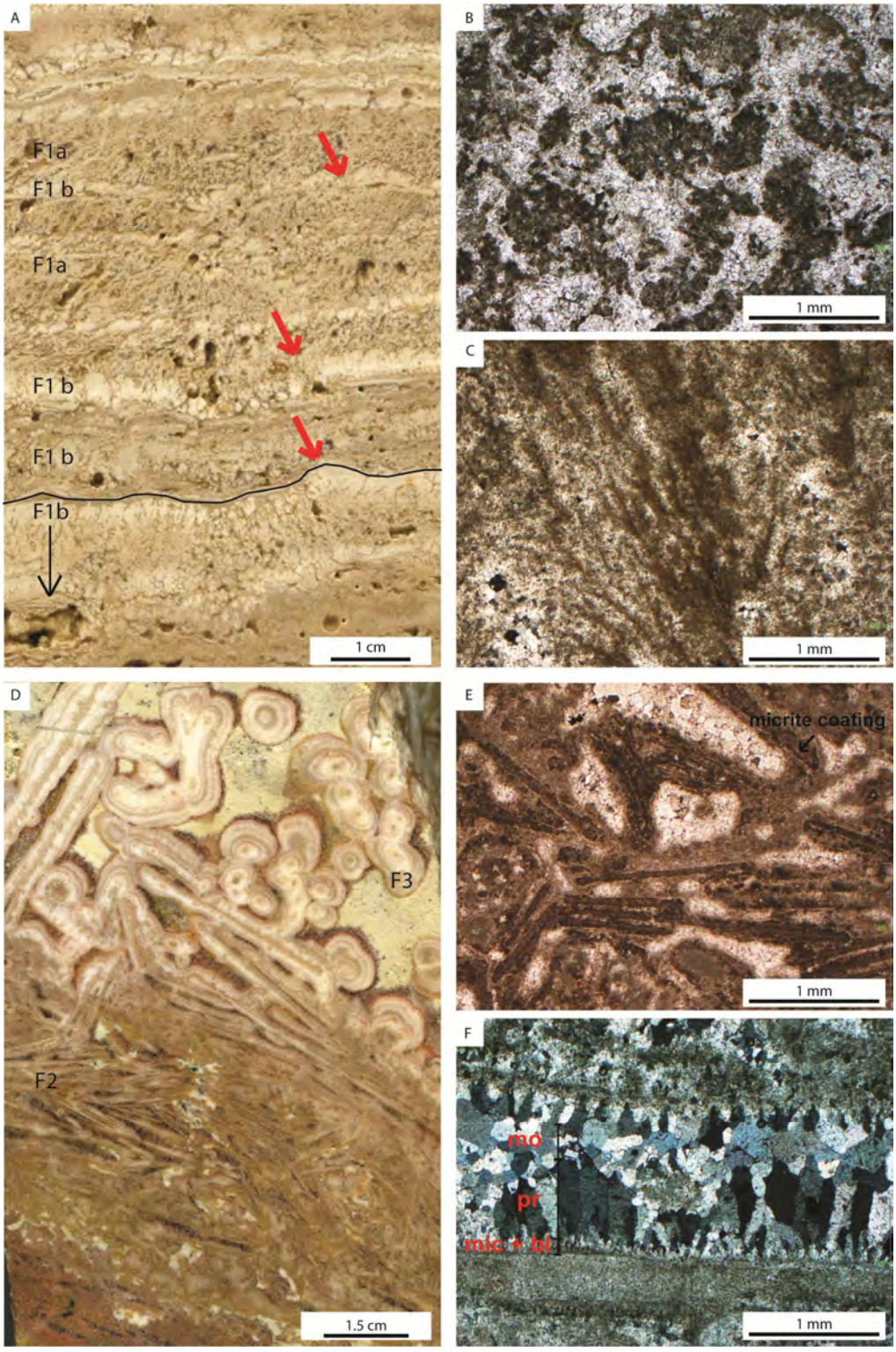

Figure 6

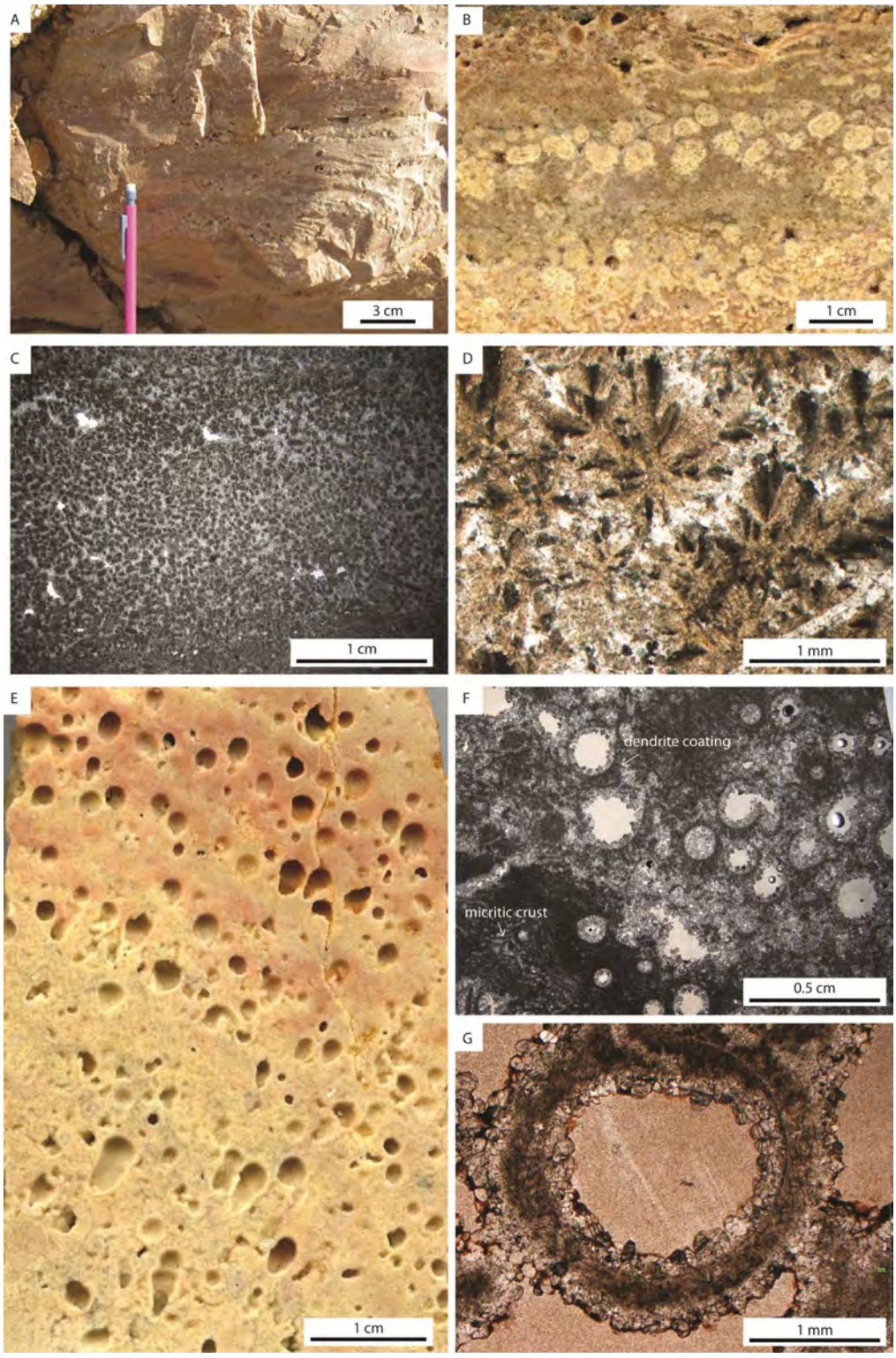

Figure 7

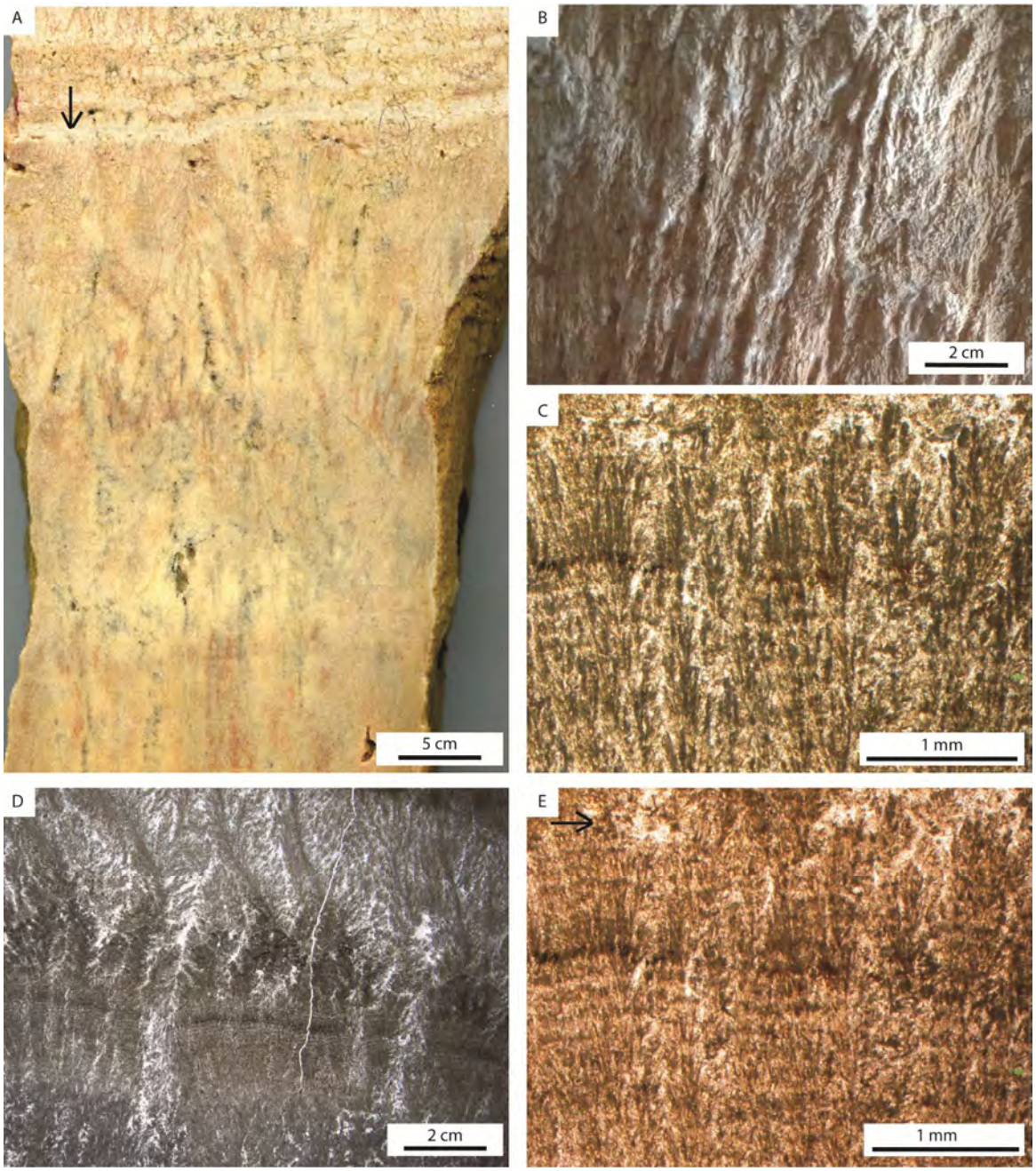

Figure 8

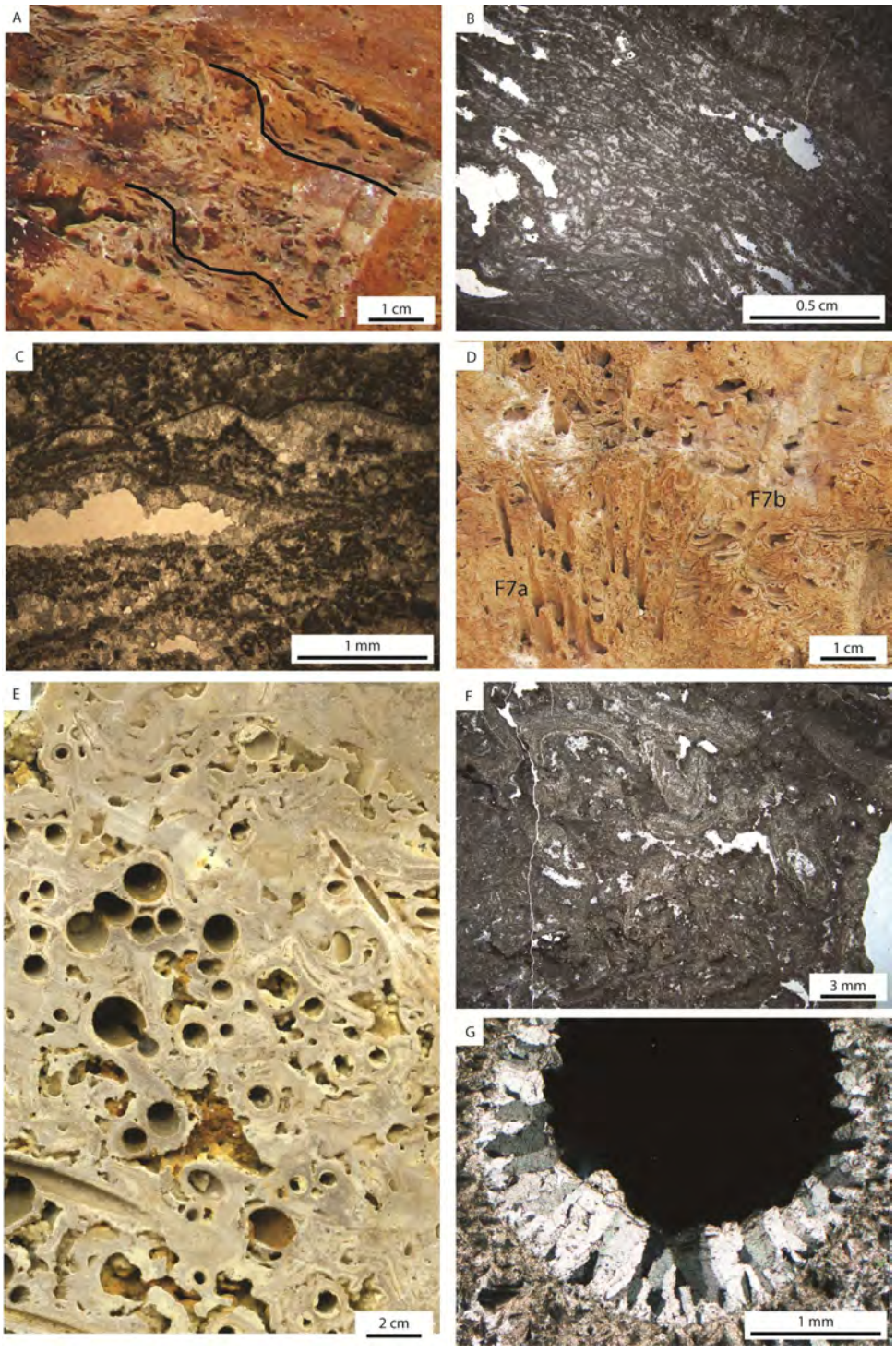

Figure 9

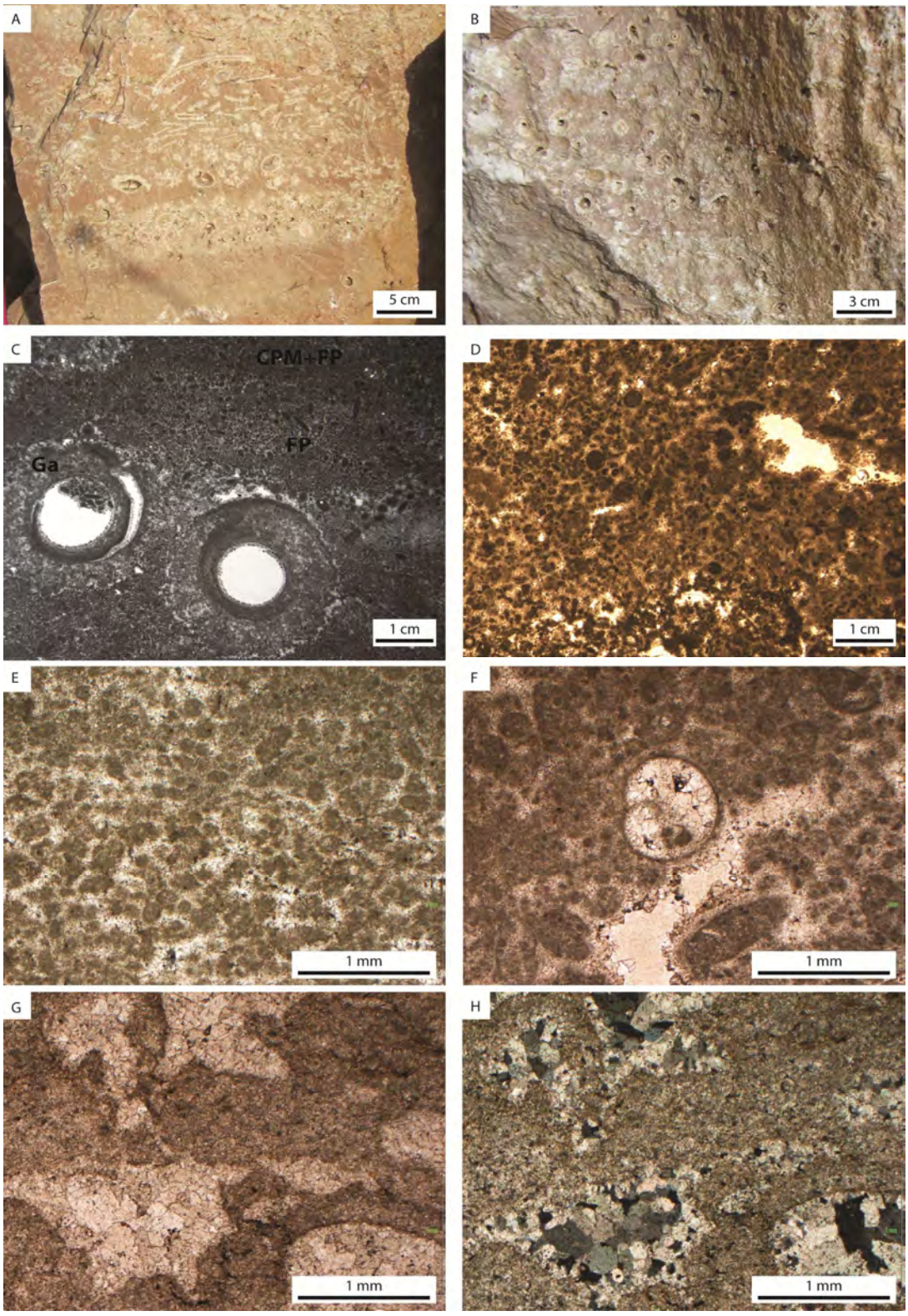

Figure 10

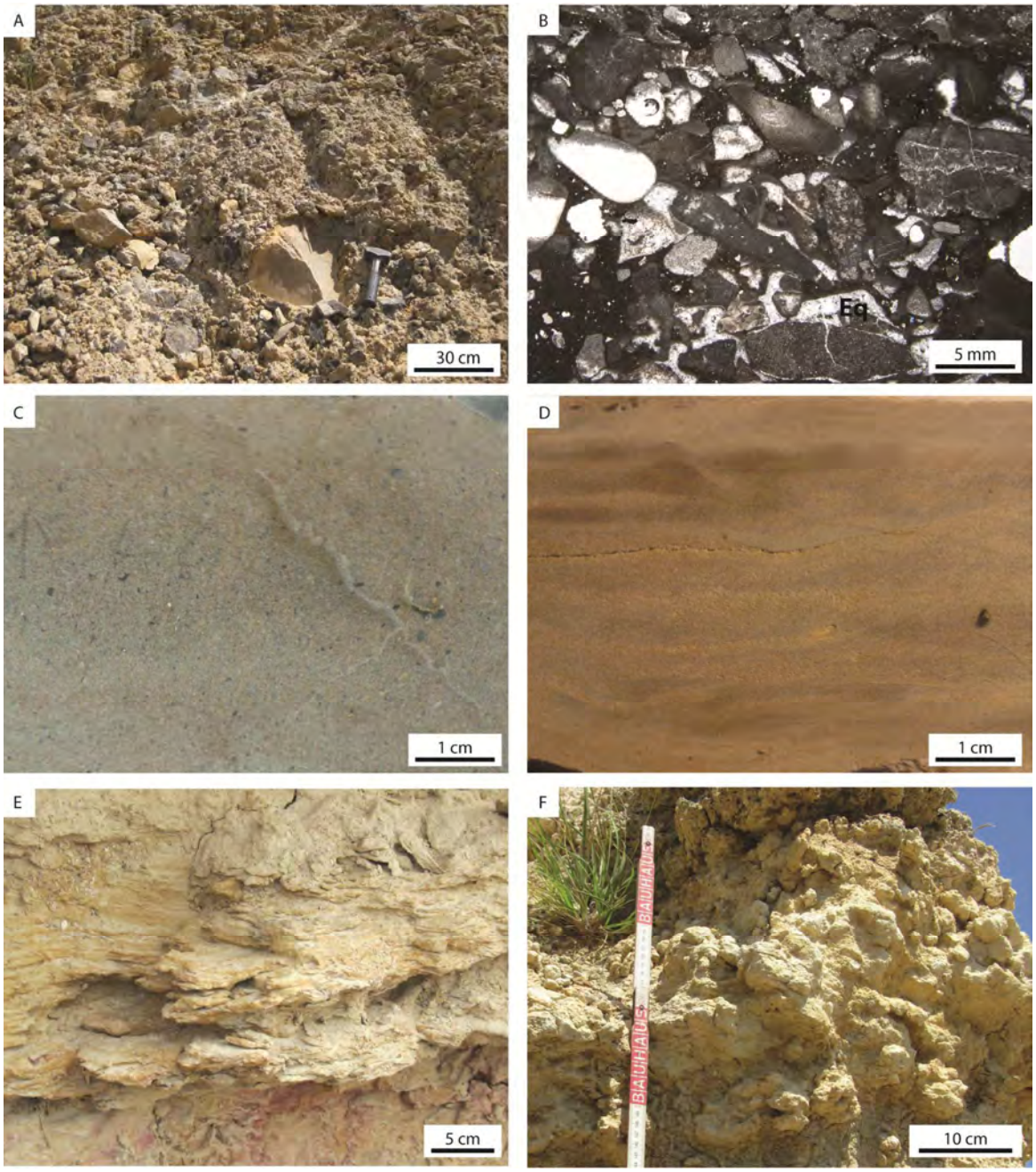

Figure 11

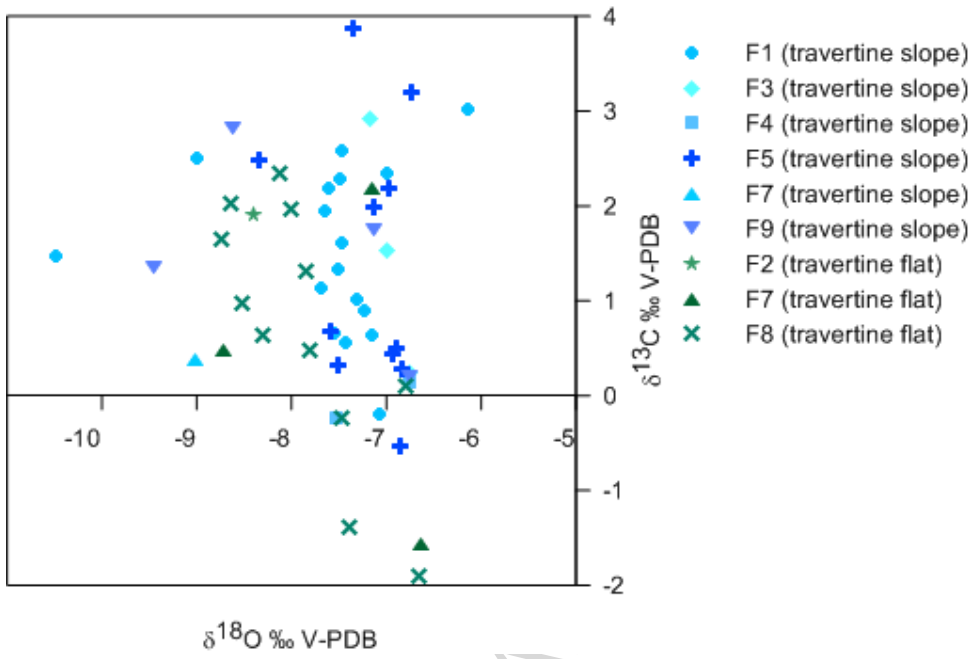

Figure 12

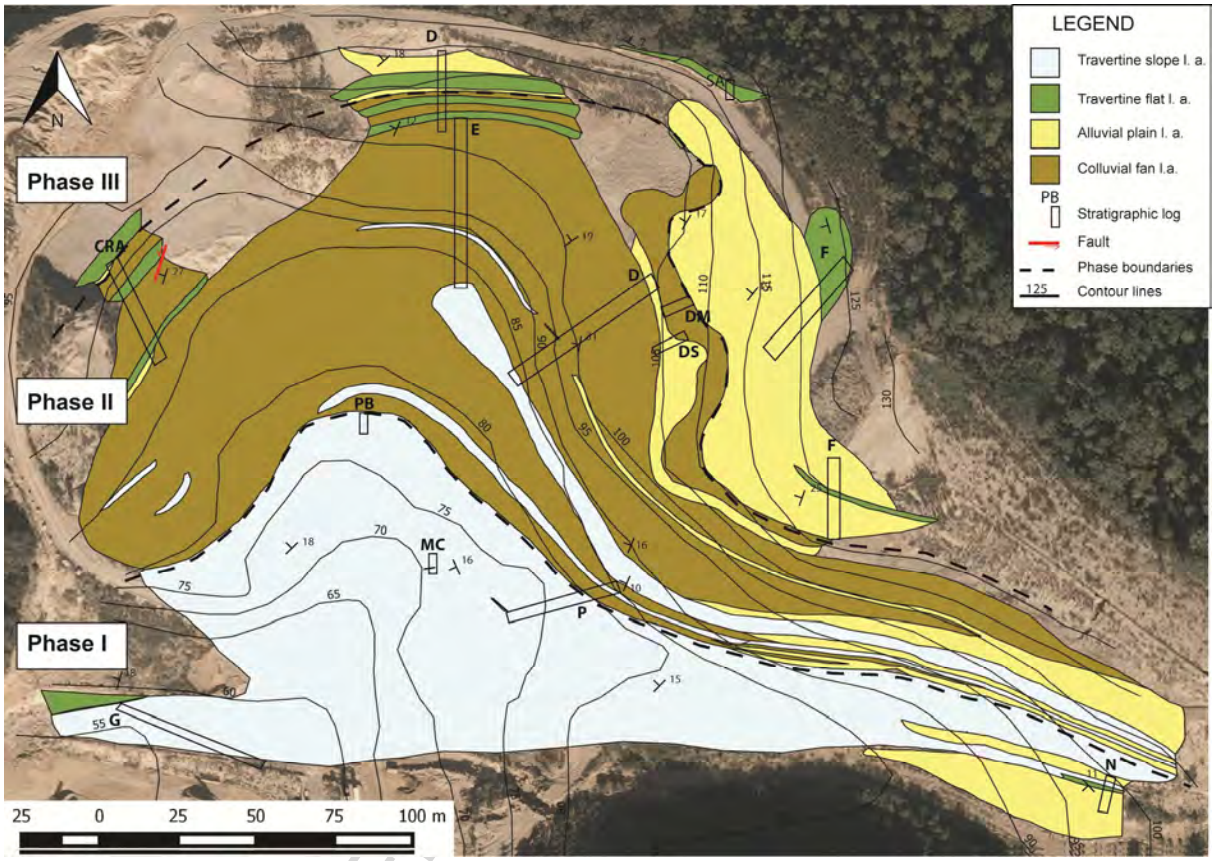

Figure 13

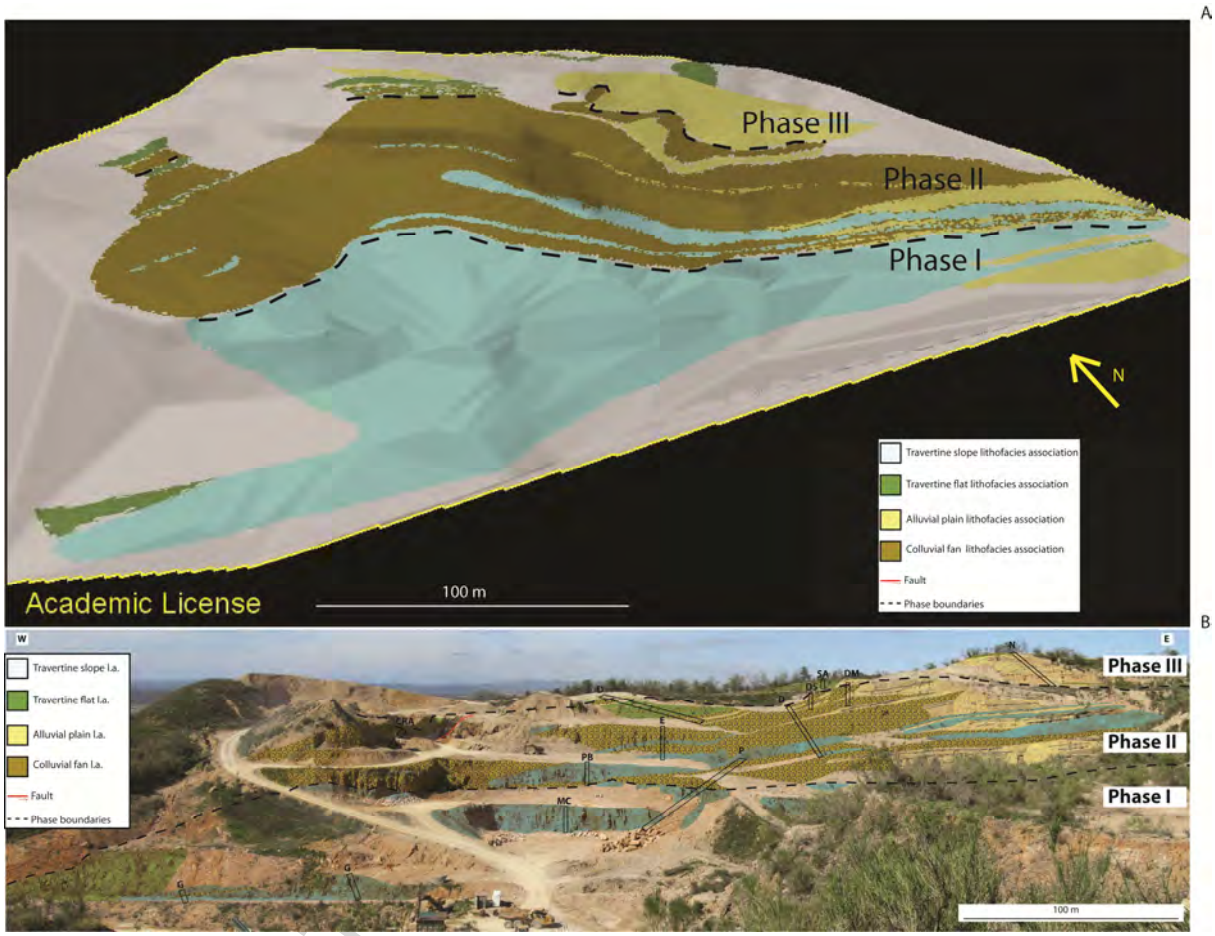

Figure 14

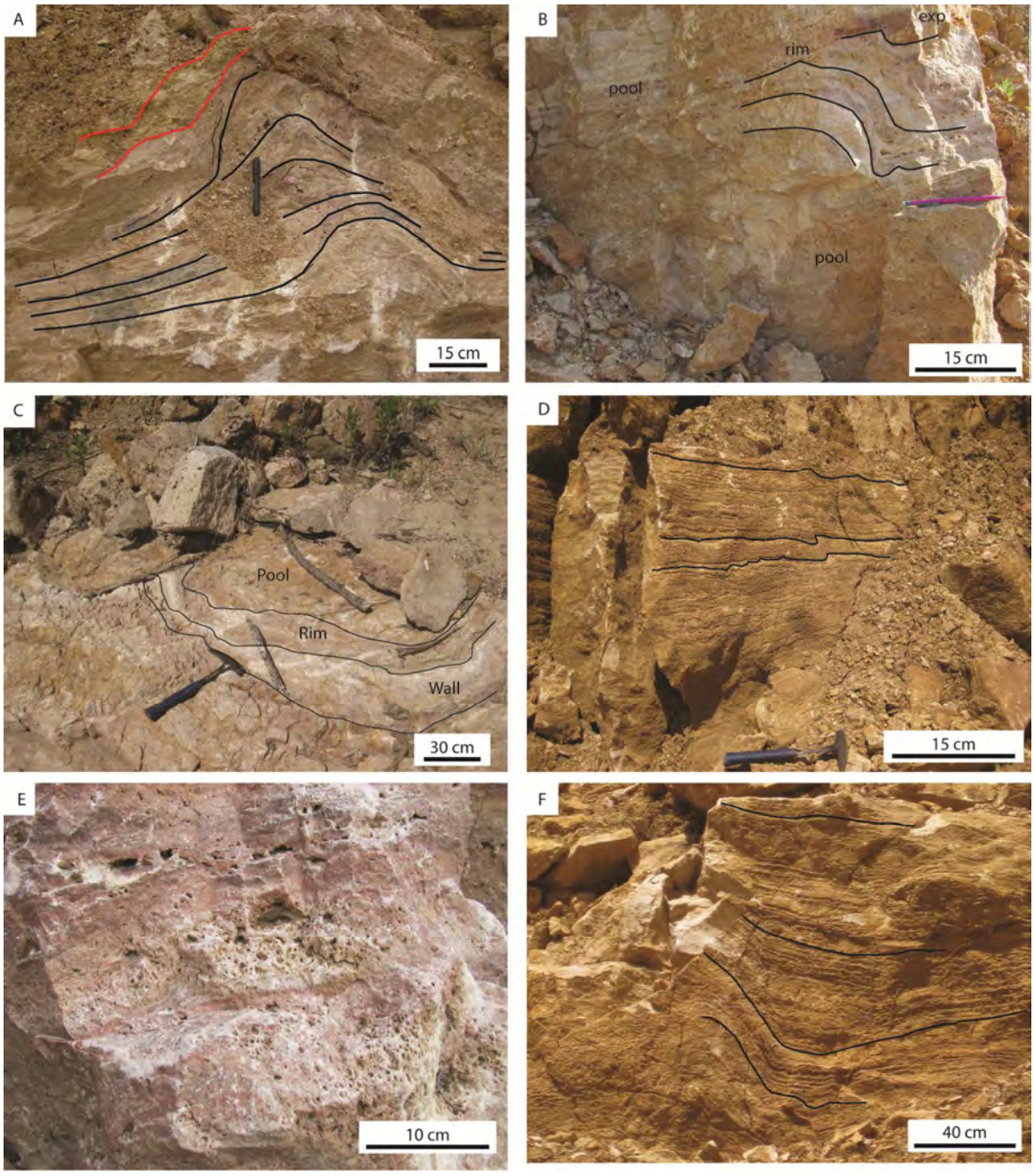

Figure 15

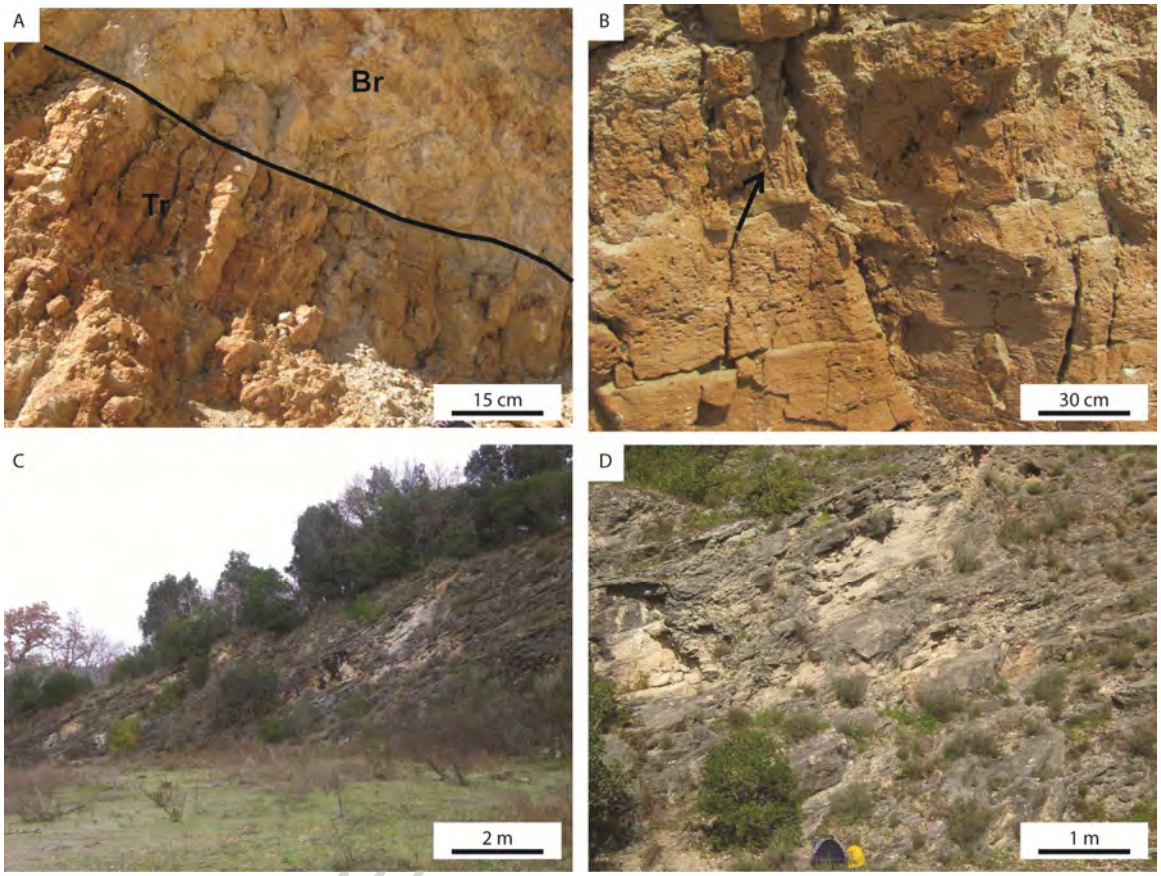

Figure 16

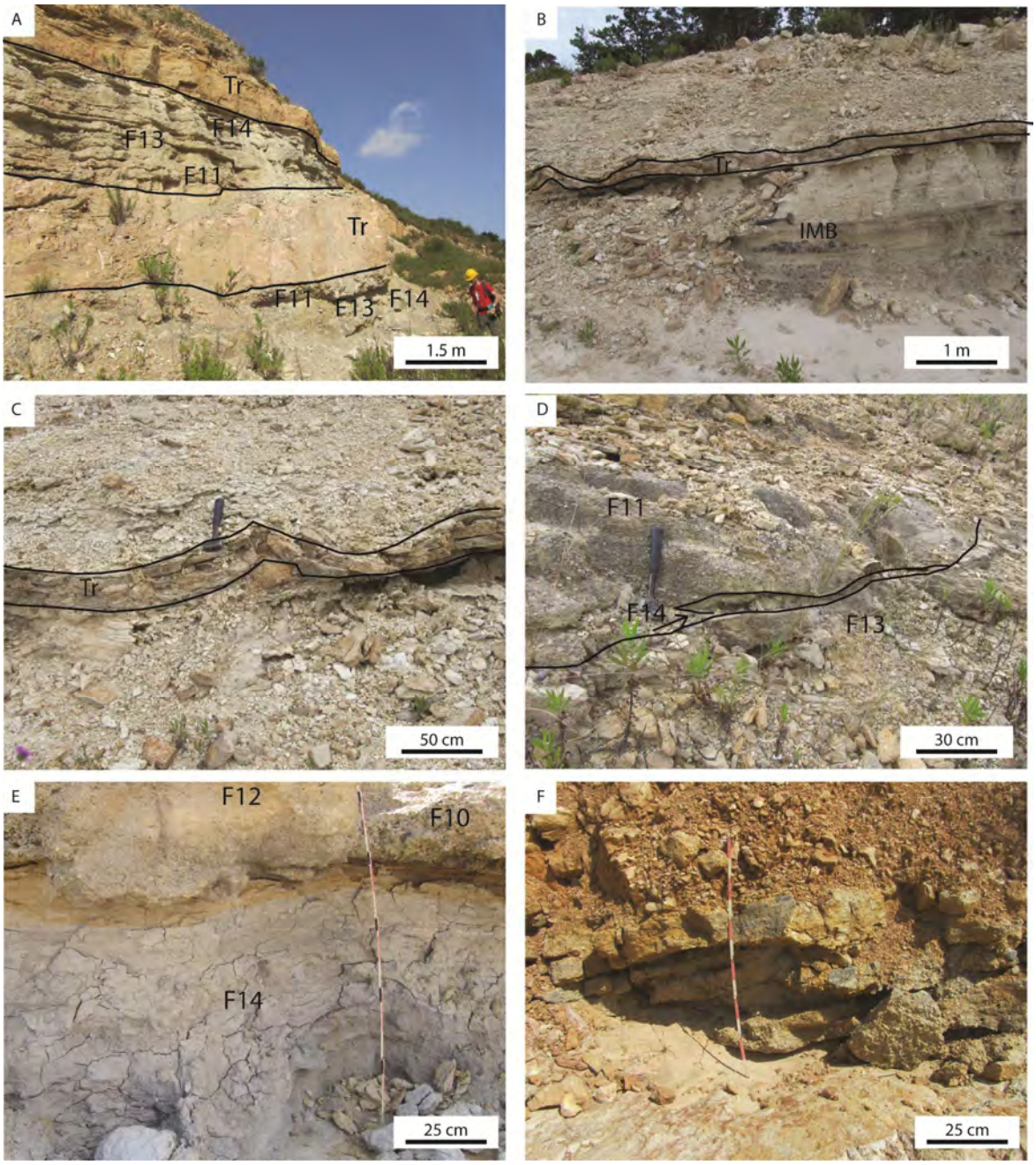

Figure 17

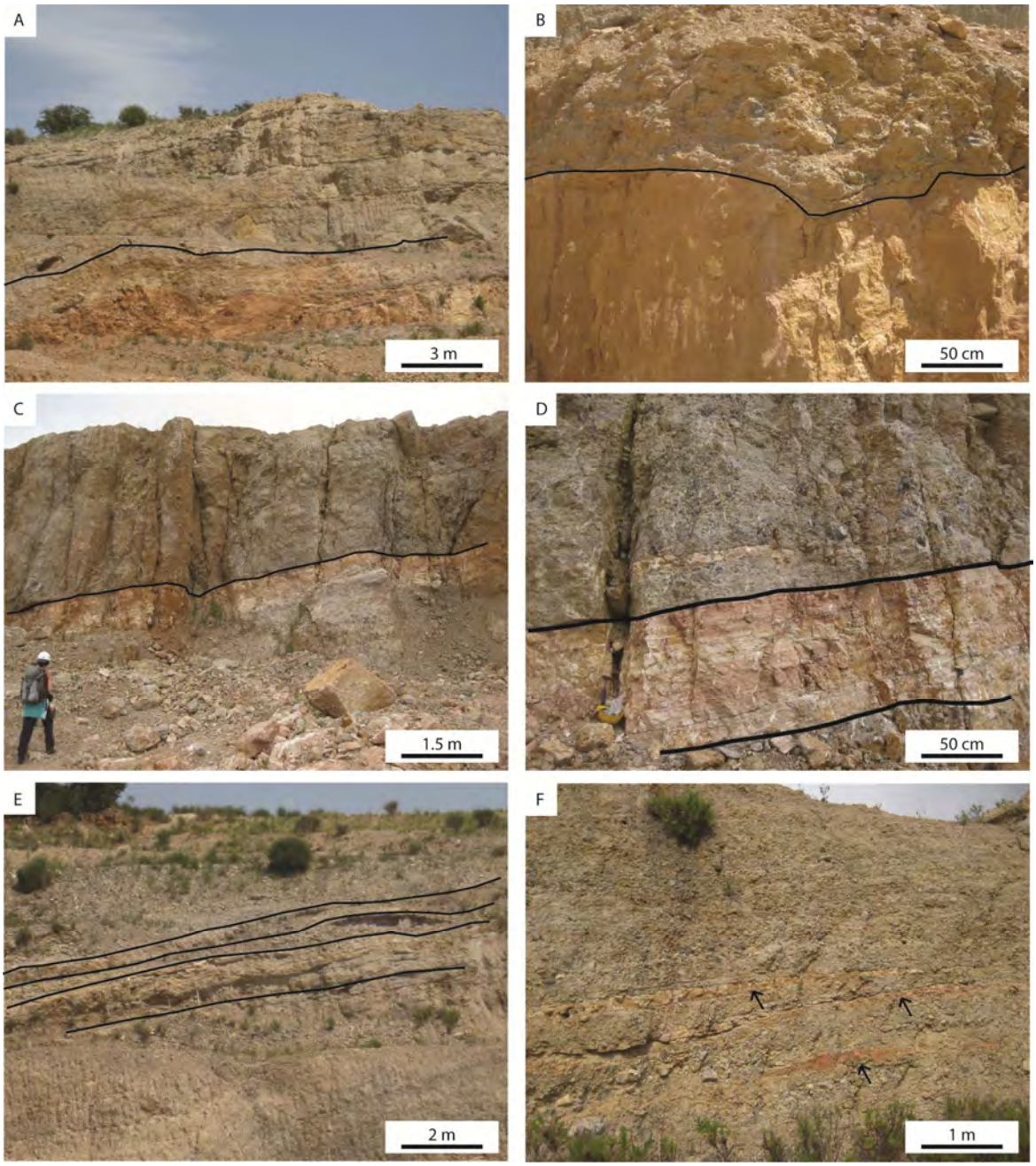

Figure 18

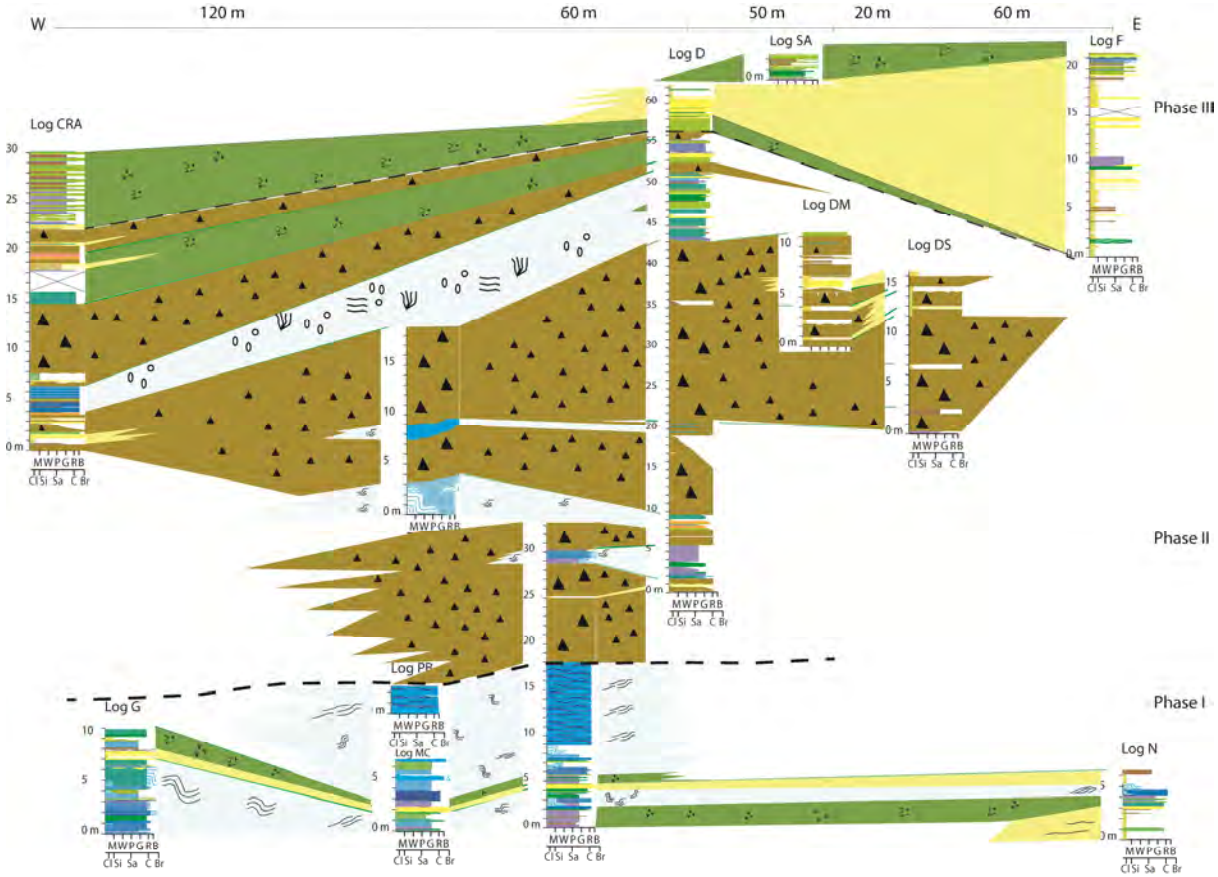

Figure 19

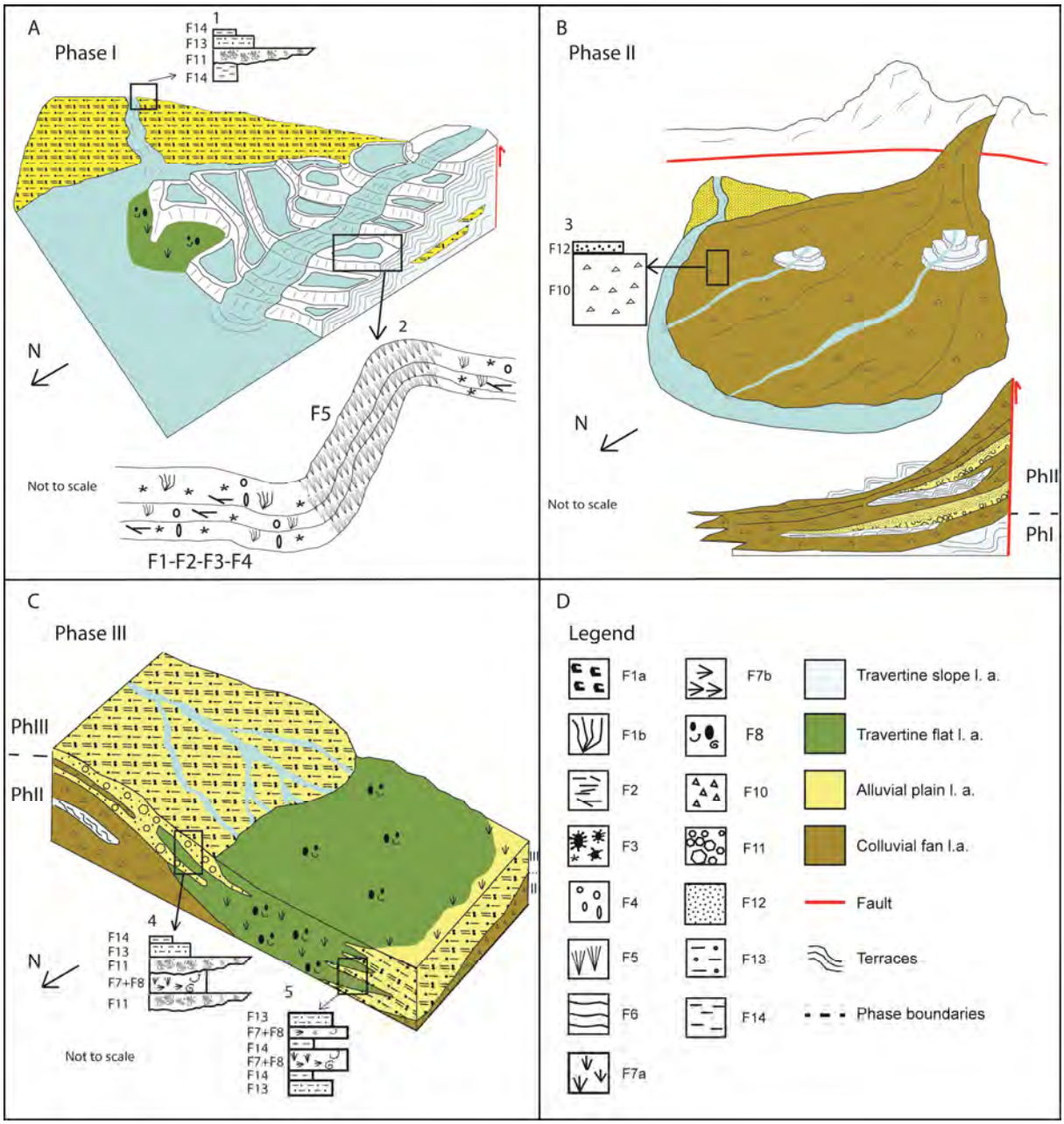

Figure 20

Table 1. Description and interpretation of travertine facies recognized in the studied succession.

Facies name and texture	Components	Bedding Thickness and Geometry	Diagenetic Features	Porosity type and %	Associated Facies	Depositional Environment	Distribution
F1a,b Clotted peloidal micrite and microsparite boundstone to grainstone	clotted peloidal micrite/10–20 µm/sub-rounded; aggregates of clotted peloidal micrite/200–300 µm/irregular; micritic dendrites up to 3 cm thick; microsparite crystals/ equant/10–20 µm; ostracodes, gastropods	undulated sub-horizontal convex shaped 0.5–10 cm	dissolution; cements: pendant (10 µm); scalenohedral (1 mm); equant (300 µm)	interparticle (100–500 µm) vuggy (100–500 µm) fenestral (0.5–1 cm) 2-5%	F1a: F2, F3, F4, F7a,b,c, F8, F9. F1b. F2, F3, F4, F7a,b	terraces and shallow pools of terraced slope system; ponds	Phase I: common Phase II: common Phase III: common
F2 Raft floatstone/rudstone	raft fragments (clotted peloidal micrite and microsparite)/200 µm thick, from mm to 5 cm in length reed moulds, gastropods, ostracodes, faecal pellets	undulated sub-horizontal 0.5–2 cm concave lenses 5–6 cm wide 2–6 cm thick	dissolution; cements: scalenohedral(600 µm); equant (300 µm)	interparticle elongated (mm up to 1 cm wide); vuggy (0.2–2 cm) 5-15%	F1a, b, F3, F4, F7b	pools of terraced slope system	Phase I: common Phase II: sparse Phase III: rare
F3 Sub-rounded radial coated grain grainstone/packstone	coated grains consist of: 1) nucleus = micrite and microsparite, faecal pellets, skeletal fragments/50–200 µm 2) radial coating = turbid calcite crystals/200–700 µm/lozenge forming spherulites microsparite/10–30 µm/equant, raft fragments	concave lenses 15–20 cm wide and 5–6 cm thick undulated sub-horizontal 1 cm	dissolution; cements: scalenohedral (200–250 µm); equant (20–30 µm)	interparticle (100–200 µm) vuggy (2 mm) 0-5%	F1a,b, F2, F4, F7b	pools of terraced slope system	Phase I: sparse Phase II: very rare Phase III: very rare
F4 Coated gas bubble boundstone	micrite/structureless aggregates of clotted peloidal micrite/50–100 µm/sub-rounded, dendrites, undulated films raft fragments	undulated sub-horizontal 3–20 cm	cements: scalenohedral (500–600 µm)	intra-bubble (from 100 µm up to 2 cm in diameter; 4 cm in length when elongated; vuggy (0.5–2 mm), 15–25 %	F2, F6, F7b	pools of terraced slope system channels	Phase I: common Phase II: common Phase III: no
F5 Crystalline dendrite cementstone	turbid calcite crystals/100–200 µm/elongate lozenge; aggregate of calcite crystals/500 µm—5 cm/fan with axial divergences of 10–30°; microsparite/10—20 µm	undulated inclined convex shaped geometries 2–15 cm	cements: microsparite/10–20 µm; replacive equant sparite	vuggy (up to 2 mm) 0–5%	F1a, F4, F6	smooth slope terraces (rim, wall)	Phase I: common Phase II: sparse Phase III: no
F6 Laminated boundstone	laminae (clotted peloidal micrite and microsparite)/50–200 µm thick/loosely to densely packed	undulated sub-horizontal horizontally wavy laminated 2–10 cm	cements: scalenohedral (300–500 µm); equant (300 µm)	inter-laminae (up to 5 cm) 0–2 % densely packed; 5–10 % loosely packed	F5, F7a,b	terraced slope system pools	Phase I: sparse Phase II: rare Phase III: no
F7a Coated reed boundstone F7b Phytoclastic rudstone/packstone	reed moulds/from mm to cm/from rounded to elongate; phytoclastic remains/30–50 µm thick, mm long/blade undulated faecal pellets, ostracodes, gastropods	undulated sub-horizontal 5–20 cm	dissolution cements: scalenohedral prismatic (200–800 µm); equant calcite (300 µm)	mouldic (up to 1 cm diameter; up to 15 cm in length); fenestral (5–7 cm) 10–20%	F7a: F1a,b, F7b, F8, F9, F10, F7b: F1a,b, F2, F3, F4	edge pools of terrace systems edge of ponds	Phase I: sparse Phase II: common Phase III: common
F8 Skeletal peloidal packstone/grainstone to floatstone/rudstone	faecal pellets/100-500 µm/rounded aggregates of clotted peloidal micrite/200–300 µm ostracodes/200 µm, gastropods/200µm–2cm phytoclastic remains, raft fragments.	undulated sub-horizontal 5–10 cm	dissolution cements: scalenohedral prismatic (300 µm) pendant (10–20 µm); equant (100–250 µm)	interparticle (200–500 µm); fenestral (up to 4 cm); intraparticle(0.5–1 mm) 5-10%	F1a, F7a, b, F9	ponds	Phase I: very rare Phase II: very rare Phase III: common
F9 Calci-mudstone to microsparstone	clotted peloidal micrite/10–20 µm/sub-rounded ; aggregates of clotted peloidal micrite/200–300 µm/irregular to dendrite; microsparite crystals/rhombic/10–20 µm; micrite/structureless	sub-horizontal 2–10 cm	dissolution cements: equant calcite (300 µm)	vuggy, channel (0.5–2 mm) 0-2%	F1a, F2, F4, F7a, b, F8	ponds	Phase I: very rare Phase II: sparse Phase III: sparse

Table 2. Description and interpretation of terrigenous facies recognized in the studied succession.

Facies name	**Bedding and structures**	**Facies thickness**	**Texture and Grain size**	**Composition**	**Sorting**	**Roundness sphericity**	**Porosity %**	**Depositional environment**	**Associated facies**
F10 Breccia	crudely bedded massive	min: 1 m max: 12 m	breccia matrix- to grain supported from mm to boulders (80 cm)	recrystallized calci-mudstone/microsparstone clasts 40–70% grey limestone clasts 10–20% fine-grained sandstone, siltstone and claystone lithic fragments 0–2% travertine intraclasts 0–2% micritic/microsparitic matrix 20–30%	very poor	angular/low sphericity	0%	colluvial fan debris flow	F12
F11 Conglomerate	horizontal bedding imbrication fining upward sequences	min: 5 cm max: 20 cm	conglomerate grain supported close framework granules and pebbles (mm to 20 cm)	recrystallized calci-mudstone/microsparstone clasts 30–70% grey limestone clasts 0–5% micritic microsparitic and clotted peloidal micrite matrix 10–20%	poor	sub-rounded/low sphericity	0–2%	channel bed lake delta	F13, F14
F12 Massive sandstone	massive weak lamination	min: 5 cm max: 20 cm	sandstone medium to coarse sand (0.25-1 mm)	detrital quartz 10–30% recrystallized calci-mudstone/microsparstone clasts 30–50% siltstone and claystone lithic fragments 10—20% micas <2%	well	angular/low sphericity	0–2%	gravity flow sedimentary sheet flood lake delta	F10, F11, F13, F14
F13 Laminated sandstone to siltstone	cross-lamination	min: 5 cm max: 80 cm	sandstone/siltstone fine sand to siltstone (0.64-250 µm)	detrital quartz 10–30% recrystallized calci-mudstone/microsparstone clasts 30–50% siltstone and claystone lithic fragments 10–20% mica <2%	well	angular/low sphericity	0–2%	abandoned channel lower flow regime	F11, F14
F14 Claystone	massive horizontal laminated	min: 5 cm max: 170 cm	clay (< 0.64 µm)		well		0%	overbank of a flood plain drape deposits freshwater ponds	F11, F12, F13, F14